J. Fluid Mech. (1996), *vol.* 325, *pp.* 79–111

The flow field due to a body in impulsive motion

By RENWEI MEI[1] AND CHRISTOPHER J. LAWRENCE[2]

[1] Department of Aerospace Engineering, Mechanics and Engineering Science, University of Florida, Gainesville, FL 32611, USA
e-mail: rwm@mozart.aero.ufl.edu

[2] Department of Chemical Engineering and Chemical Technology, Imperial College of Science, Techology and Medicine, London SW7 2BY, UK
e-mail: c.lawrence@ic.ac.uk

(Received 2 November 1995 and in revised form 20 May 1996)

An asymptotic analysis for the long-time unsteady laminar far wake of a bluff body due to a step change in its travelling velocity from U_1 to U_2 is presented. For $U_1 \geqslant 0$ and $U_2 > 0$, the laminar wake consists of a new wake of volume flux Q_2 corresponding to the current velocity U_2, an old wake of volume flux Q_1 corresponding to the original velocity U_1, and a transition zone that connects these two wakes. The transition zone acts as a sink (or a source) of volume flux $(Q_2 - Q_1)$ and is moving away from the body at speed U_2. Streamwise diffusion is negligible in the new and old wakes but a matched asymptotic expansion that retains the streamwise diffusion is required to determine the vorticity transport in the transition zone. A source of volume flux Q_2 located near the body needs to be superposed on the unsteady wake to form the global flow field around the body. The asymptotic predictions for the unsteady wake velocity, unsteady wake vorticity, and the global flow field around the body agree well with finite difference solutions for flow over a sphere at finite Reynolds numbers. The long-time unsteady flow structures due to a sudden stop ($U_2 = 0$) and an impulsive reverse ($U_1 U_2 < 0$) of the body are analysed in detail based on the asymptotic solutions for the unsteady wakes and the finite difference solutions. The elucidation of the long-time behaviour of such unsteady flows provides a framework for understanding the long-time particle dynamics at finite Reynolds number.

1. Introduction

In a recent paper (Lawrence & Mei 1995, hereinafter referred to as LM), the long-time unsteady force on a moving bluff body due to a step change in its velocity from U_1 to U_2 was obtained at finite Reynolds number, Re. The step change in the velocity includes a sudden change of velocity from $U_1(>0)$ to $U_2(>0)$, an impulsive start from $U_1 = 0$ to $U_2 > 0$, a sudden stop from U_1 to $U_2 = 0$, and an impulsive reverse from $U_1 < 0$ to $U_2 > 0$. It was shown that for the sudden increase (or decrease) and the impulsive start, the long-time transient force decays as t^{-2} at finite Reynolds number because a sink, whose strength is proportional to the difference in the respective steady wake volume fluxes $(Q_2 - Q_1)$, moves away from the body at speed U_2 along the wake. The transient force decays as t^{-1} for the impulsive stop and reverse because the body is immersed in the wake it previously created and the wake velocity decays as x^{-1} in the streamwise (x) direction. These simple asymptotic results compare very well with carefully obtained finite difference results for the long-time unsteady force on a sphere. The results also agree with the low-Reynolds-number results of Lovalenti & Brady (1993), who used a reciprocal theorem and point-force formulation for the impulsive

start, impulsive stop and impulsive reverse. The t^{-2} decay of the transient force at finite Reynolds number for the case of sudden change of velocity from $U_1 > 0$ to $U_2 > 0$ is also in excellent agreement with the more recent, and more accurate, low-Reynolds-number analytical result (Lovalenti & Brady 1995).

Since the results for the long-time transient force obtained by LM and by Hinch (see Lovalenti & Brady 1993) were obtained by very simple arguments based on the gross features of the unsteady wake, detailed analyses for the unsteady flow field are thus necessary to gain further understanding of particle dynamics at finite Reynolds number. In this paper we present a long-time asymptotic analysis for the unsteady wake structure behind a bluff body. A global approximation for the entire flow field is then obtained based on superposition of linear flow elements. The asymptotic flow field is compared with detailed numerical results for flow around a sphere at Reynolds numbers up to 60; very good agreement is obtained over the whole flow field apart from a small near-wake region where nonlinear interaction is clearly important. The details of the flow structure, especially those revealed by the asymptotic analysis, shed much light on the nature of the unsteady laminar wake of a bluff body and the details of vorticity transport in those unsteady flows.

We consider a body of characteristic radius a moving in a fluid of kinematic viscosity ν and density ρ toward the left with the centre of the coordinates attached to it. For a zero-thickness plate or disk placed normal to the flow, the characteristic dimension of the body should be a typical radius or width. The wake may be regarded as the region containing the vorticity generated at the surface of the body. This vorticity spreads out owing to diffusion as it is swept downstream by the mean flow, so the steady wake is parabolic in geometry, as well as mathematically. Since the vorticity is zero on the axis and far away from it, the wake may be thought of as forming a 'pipe' which both confines and conveys a flux towards the body. In a steady flow, this wake flux is a constant proportional to the drag on the body. After the body changes its velocity from U_1 to U_2 at $t = 0$, the flow field behind the body at large times consists of a new wake ($0 < x < U_2 t$) and an old wake ($x > U_2 t$) connected by a transition zone of size $(\nu t)^{1/2}$ at $x \sim U_2 t$, as shown in figure 1(*a*). The new wake is quasi-steady in the coordinate frame attached to the body, whereas the old wake is not. The old wake would be quasi-steady in a frame moving at speed $(U_2 - U_1)$, so we say that the old wake is moving at speed $(U_2 - U_1)$. The old wake is gradually overtaken by the transition zone moving at speed U_2. The flow in the transition zone is both unsteady in time and elliptic in space. The physical significance of the transition zone, when viewed far away from it, is a sink whose strength is proportional to the difference in the respective steady wake volume fluxes $(Q_2 - Q_1)$. Asymptotic solutions for the flow in these three regions of the far wake can be obtained. Matching is accomplished between the new wake and the transition zone and between the transition zone and the old wake. An analytical approximation for the global flow field is subsequently obtained by further superimposing a source of volume flux Q_2 at $x = 0$ to maintain the global mass balance. The full unsteady flow field is also obtained by solving the Navier–Stokes equation using a finite difference method, which is a refinement of that used by Mei (1993). Excellent agreement is observed for the wake velocity and the off-centreline vorticity between the numerical solution and matched asymptotic solution for a sudden increase in velocity ($Re_1 = 40$, $Re_2 = 60$).

For an impulsive start ($U_1 = 0$), the asymptotic and numerical solutions for the flow field reveal the following simple, large-scale features: a dipole is created at $t = 0$ when the body is impulsively started; the dipole is then stretched out with the source attached to the body moving to the left at velocity U_2 leaving a sink of the same strength at a

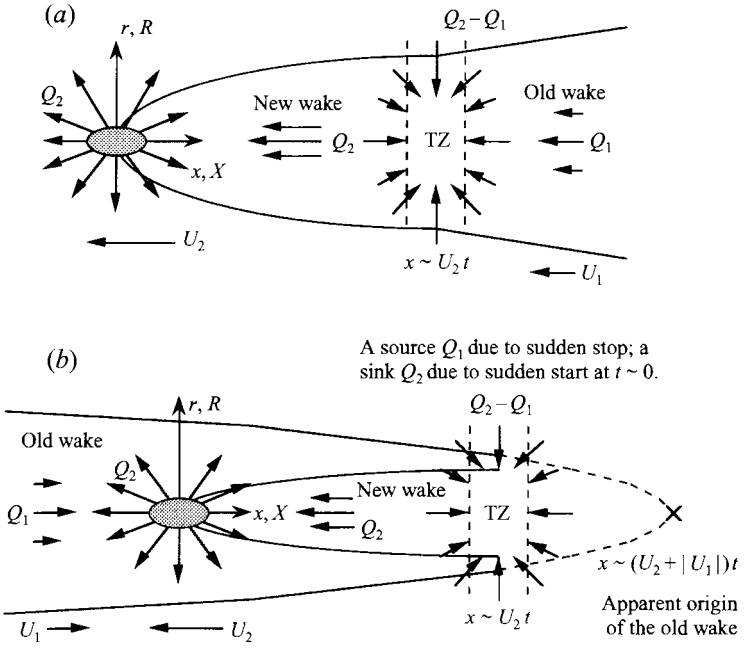

FIGURE 1. Principal features of the unsteady wake at large times due to (*a*) a step change from U_1 to U_2 in the velocity of the body, and (*b*) a sudden reverse from U_1 to U_2 ($U_1 U_2 < 0$) in the velocity of the body, both at $t = 0$. TZ denotes transition zone.

distance $x \sim U_2 t$ behind it; between the source and the sink lies a new wake. The global flow field obtained from the simple analytical approximation agrees well with that from the numerical solution for the impulsive-start case (at $Re_2 = 40$).

The global flow field due to a sudden stop contains the old steady wake of volume flux Q_1 that travels toward the body and a diffusing source of flux Q_1 centred on the body. The body thus sees a temporally decaying, spatially decelerating flow around it. In the impulsive reverse case, the body moves to the right with velocity $U_1 < 0$ for $t < 0$ and then moves to the left with velocity $U_2 > 0$ for $t > 0$. The long-time global flow field can be considered to result from two impulsive processes: an impulsive stop of the body with velocity changing from U_1 to 0 at $t = 0^-$; and subsequently an impulsive start of the body with velocity changing from 0 to U_2 to $t = 0^+$. Thus, the global flow field has the following principal flow elements: (*a*) an old wake with its apparent origin moving at $x \sim (U_2 - U_1)t$; (*b*) a diffusing source of volume flux Q_1 at $x \sim U_2 t$; (*c*) a new source of volume flux Q_2 at $x \sim 0$; (*d*) a new wake of flux Q_2 in $0 < x < U_2 t$; and (*e*) a new sink of volume flux Q_2 at $x \sim U_2 t$. The first two elements and the last three elements are associated, respectively, with the impulsive stop and impulsive start. The detailed finite difference solutions for flow over a sphere confirm the analysis of the global flow field due to the impulsive stop and reverse of the body. The asymptotic results are, however, valid for arbitrary body geometry which does not generate lift.

The asymptotic analyses for the unsteady far wake due to the sudden change in velocity are presented in §§2.1–2.3. In §2.4 we extend the asymptotic analysis to the flow due to an impulsive stop. The description of the flow due to an impulsive reverse is given in §2.5. The finite difference procedure is briefly summarized in §3. Results and further discussion of the unsteady flow fields are presented in §4.

2. Asymptotic analyses for the unsteady flow fields

2.1. *Basic equations*

For mathematical convenience, we attach the coordinates to the centre of the moving bluff body of characteristic radius a and consider a uniform flow past the body. In the case of sphere, a is the radius of the sphere. The flow is assumed to be axisymmetric, incompressible, and laminar. At this point, we primarily focus on the flow field in the far-wake region, $x \gg a$. In cylindrical polar coordinates (x, r, φ), the governing equations for the velocity $\boldsymbol{u} = u\boldsymbol{e}_x + v\boldsymbol{e}_r = (u, v, 0)$ are

$$u_x + v_r + \frac{1}{r}v = 0, \tag{1}$$

$$u_t + uu_x + vu_r = -\frac{1}{\rho}p_x + \left(u_{xx} + u_{rr} + \frac{1}{r}u_r\right), \tag{2}$$

$$v_t + uv_x + vv_r = -\frac{1}{\rho}p_r + \nu\left(v_{xx} + v_{rr} + \frac{1}{r}v_r - \frac{1}{r^2}v\right), \tag{3}$$

where the subscripts t, x, and r denote the partial derivatives with respect to the corresponding variable. The equations governing the transport of the vorticity $\omega = v_x - u_r$ and the stream function are

$$\omega_t + u\omega_x + v\omega_r - \frac{1}{r}v\omega = \nu\left(\omega_{xx} + \omega_{rr} + \frac{1}{r}\omega_r - \frac{1}{r^2}\omega\right), \tag{4}$$

$$\psi_{xx} + \psi_{rr} - \frac{1}{r}\psi_r = -r\omega. \tag{5}$$

The boundary conditions for flow past the fixed body are

$$\left.\begin{aligned} &\boldsymbol{u} = 0 \text{ on the body,} \\ &u = U(t), \quad v = 0, \quad p = p_\infty \quad \text{as} \quad x^2 + r^2 \to \infty. \end{aligned}\right\} \tag{6}$$

Of particular interest is the response of the flow to the velocity variation

$$U(t) = \begin{cases} U_1 & \text{for} \quad t < 0 \\ U_2 & \text{for} \quad t > t_2, \end{cases} \tag{7}$$

in which U_1 and U_2 are constants, and t_2 is of $O(a/U_2)$. Any reasonable transition from U_1 to U_2 would yield the same asymptotic results at large times. In the numerical computation for flow over a sphere, t_2 is simply taken to be zero.

Introducing the scales

$$U_2, \quad \rho U_2^2, \quad U_2/a, \quad U_2 a^2, \quad a, \quad a/U_2 \tag{8}$$

to normalize the variables

$$\boldsymbol{u}, \quad p - p_\infty, \quad \omega, \quad \psi, \quad (x, r), \quad t, \tag{9}$$

the following dimensionless equations are obtained:

$$u_x + v_r + \frac{1}{r}v = 0, \tag{10}$$

$$u_t + uu_x + vu_r = -p_x + \frac{1}{Re'}\left(u_{xx} + u_{rr} + \frac{1}{r}u_r\right), \tag{11}$$

$$v_t + uv_x + vv_r = -p_r + \frac{1}{Re'}\left(v_{xx} + v_{rr} + \frac{1}{r}v_r - \frac{1}{r^2}v\right), \tag{12}$$

$$\omega_t + u\omega_x + v\omega_r - \frac{1}{r}v\omega = \frac{1}{Re'}\left(\omega_{xx} + \omega_{rr} + \frac{1}{r}\omega_r - \frac{1}{r^2}\omega\right). \tag{13}$$

The dimensionless boundary conditions are

$$\boldsymbol{u} = 0 \quad \text{on the body}$$

$$v = 0, \quad p = 0, \quad \text{and} \quad u = U = \begin{cases} \alpha_{12} & \text{for} \quad t < 0 \\ 1 & \text{for} \quad t < t_2^* \end{cases} \quad \text{as} \quad x^2 + r^2 \to \infty \tag{14}$$

with

$$Re' = U_2 a/\nu, \quad \alpha_{12} = U_1/U_2, \quad t_2^* = t_2 U_2/a. \tag{15}$$

The dimensionless equation for ψ is the same as given by equation (5).

2.2. *Wake region*

We consider a region 'far downstream' of the body, $x \gg 1$, where the wake is weak, wide and axisymmetric (cf. Batchelor 1967, p. 349). For convenience, a small parameter ϵ is introduced to characterize the 'farness' and we formally define

$$x = \frac{1}{\epsilon}X \quad \text{with} \quad X \sim O(1), \quad \epsilon \ll 1. \tag{16}$$

For consistency, other variables must be re-scaled as follows:

$$\left.\begin{aligned} &t = \frac{1}{\epsilon}T, \quad r = (\epsilon Re')^{-1/2}R, \quad u = U + \epsilon\hat{u}, \quad v = \epsilon^{3/2}Re'^{-1/2}\hat{v}, \\ &p = \epsilon^2 Re'^{-1}\hat{p}, \quad \omega = \epsilon^{3/2}Re'^{1/2}\hat{\omega}, \quad \psi = \tfrac{1}{2}r^2 + Re'^{-1}\hat{\psi}. \end{aligned}\right\} \tag{17}$$

The equations rescaled for the unsteady far wake are then obtained:

$$\hat{u}_X + \hat{v}_R + \frac{1}{R}\hat{v} = 0, \tag{18}$$

$$\hat{u}_T + U\hat{u}_X + \epsilon(\hat{u}\hat{u}_X + \hat{v}\hat{u}_R) = \hat{u}_{RR} + \frac{1}{R}\hat{u}_R + \frac{\epsilon}{Re'}(\hat{u}_{XX} - \hat{p}_X), \tag{19}$$

$$\hat{v}_T + U\hat{v}_X + \epsilon(u\hat{v}_X + \hat{v}\hat{v}_R) = -\hat{p}_R + \hat{v}_{RR} + \frac{1}{R}\hat{v}_R - \frac{1}{R^2}\hat{v} - \frac{\epsilon}{Re'}\hat{v}_{XX}, \tag{20}$$

$$\hat{\omega}_T + U\hat{\omega}_X + \epsilon\left(\hat{u}\hat{\omega}_X + \hat{v}\hat{\omega}_R - \frac{1}{R}\hat{v}\hat{\omega}\right) = \hat{\omega}_{RR} + \frac{1}{R}\hat{\omega}_R - \frac{1}{R^2}\hat{\omega} + \frac{\epsilon}{Re'}\hat{\omega}_{XX}, \tag{21}$$

$$\hat{\psi}_{RR} - \frac{1}{R}\hat{\psi}_R + \frac{\epsilon}{Re'}\hat{\psi}_{XX} = -R\hat{\omega}. \tag{22}$$

2.2.1. *Leading-order problem*

At leading order, $\epsilon \ll 1$, we simply drop $O(\epsilon)$ and $O(\epsilon/Re')$ terms, formally requiring $\epsilon \ll Re'$, to obtain

$$\hat{u}_X + \hat{v}_R + \frac{1}{R}\hat{v} = 0, \tag{23}$$

$$\hat{u}_T + U\hat{u}_X = \hat{u}_{RR} + \frac{1}{R}\hat{u}_R, \tag{24}$$

$$\hat{v}_T + U\hat{v}_X = -\hat{p}_R + \hat{v}_{RR} + \frac{1}{R}\hat{v}_R - \frac{1}{R^2}\hat{v}, \tag{25}$$

$$\hat{\omega}_T + U\hat{\omega}_X = \hat{\omega}_{RR} + \frac{1}{R}\hat{\omega}_R - \frac{1}{R^2}\hat{\omega}, \tag{26}$$

with

$$\hat{u} = 0, \quad \hat{v} = 0, \quad \hat{p} = 0, \quad \text{and} \quad \hat{\omega} = 0, \quad \text{as} \quad X^2 + R^2 \to \infty. \tag{27}$$

It is observed that the equations for $\hat{u}$ and $\hat{\omega}$ are decoupled and have a very similar structure to the leading order, $\hat{v}$ can be found from the continuity equation, and $\hat{p}$ can be found from the radial momentum equation.

2.2.2. *Steady-state wake*

By dropping the time-derivative terms in the above, the steady-state equations are obtained. For $\hat{u}$ and $\hat{\omega}$, the resulting equations are simple convection–diffusion equations of parabolic type with constant convective speed and homogeneous boundary conditions. Following Schlichting (1979, p. 234) and Batchelor (1967, p. 349), the solution for $\hat{u}$ is

$$\hat{u}(X, R) = -\frac{\hat{Q}}{4\pi}\frac{U}{X - X_0}\exp\left[-\frac{R^2 U}{4(X - X_0)}\right], \tag{28}$$

where X_0 is the apparent origin of the wake and

$$\hat{Q} = Q/\nu a \tag{29a}$$

in which Q is the dimensional wake volume flux that is directly related to the drag on the body. If the uniform flow velocity is U_2, the drag is then $D_2 = \rho U_2 Q_2$. Using $D_2 = 6\pi\rho\nu U_2 a\phi_2$ for a sphere in which ϕ accounts for the deviation from the Stokes drag law at finite Reynolds number (LM), we obtain

$$\hat{Q}_2 = 6\pi\phi_2. \tag{29b}$$

The vorticity can be simply obtained as

$$\hat{\omega}(X, R) = -\hat{u}_R = -\frac{\hat{Q}}{8\pi}\frac{RU^2}{(X - X_0)^2}\exp\left[-\frac{R^2 U}{4(X - X_0)}\right]. \tag{30}$$

The radial velocity is obtained from the continuity equation as

$$\hat{v}(X, R) = -\frac{\hat{Q}}{8\pi}\frac{RU}{(X - X_0)^2}\exp\left[-\frac{R^2 U}{4(X - X_0)}\right]. \tag{31}$$

It is also noted that $\hat{v}(X, R) = U\hat{\omega}(X, R)$. Finally, the pressure can be obtained from the radial momentum equation. The radial component of the pressure gradient is

$$\hat{p}_R = \left(\frac{\partial^2}{\partial R^2} + \frac{1}{R}\frac{\partial}{\partial R} - \frac{1}{R^2} - U\frac{\partial}{\partial X}\right)\hat{v} = 0 \tag{32}$$

because the operator in front of $\hat{v}$ is identical to the operator for $\hat{\omega}$ (see equations (25)–(26)) while $\hat{v} = U\hat{\omega}$. Hence, from the boundary condition at $R \to \infty$,

$$\hat{p}(X, R) = 0. \tag{33}$$

The stream function $\hat{\psi}(X, R)$ is obtained by integrating $R\hat{u}(X, R)$ with respect to R:

$$\hat{\psi}(X, R) = -\frac{\hat{Q}}{2\pi}\left\{1 - \exp\left[-\frac{R^2 U}{4(X - X_0)}\right]\right\}. \tag{34a}$$

To maintain the global mass balance, there must be a source of dimensionless volume flux $\hat{Q}$ at X_s (near $X = 0$; see Batchelor 1967, p. 351) so the global flow field is approximated as

$$\hat{\psi}(X, R) = \frac{\hat{Q}}{2\pi}\exp\left[-\frac{R^2 U}{4(X - X_0)}\right]H(x) - \frac{\hat{Q}}{4\pi}\left\{1 + \frac{X - X_s}{[(X - X_s)^2 + R^2]^{1/2}}\right\}, \tag{34b}$$

where $H(x)$ is the Heaviside unit step function taking the values zero for negative arguments and unity for positive arguments. There is no physical discontinuity in $\hat{\psi}$ as long as $X_0 < 0$ and X_s is within the body. Since the body is located at $x = 0$, we would expect X_0 and X_s to be zero. In a strict asymptotic sense, this is indeed the case for the steady solution. Nevertheless we retain X_0 and X_s because they will be relevant in constructing the unsteady solution in the old wake. Furthermore, it is our intention to compare the asymptotic solution to a numerical solution, necessarily generated for finite values of x and Re'. In that comparison, it is useful to regard X_0 and X_s as $O(\epsilon)$ adjustable parameters that account in part for higher-order terms neglected in the asymptotic analysis. In this regard, as long as X_0 and X_s are $O(\epsilon)$, or equivalently, $x_0 = X_0/\epsilon$ is $O(1)$, it is to be expected that x_0 may take different values in the velocity and vorticity solutions.

For $T < 0$, we set $U = \alpha_{12}$ in the above to obtain the steady-state wake (or old wake) solutions for $\hat{u}$, $\hat{v}$ and $\hat{\omega}$. For $T > 0$, the new steady wake is obtained by setting $U = 1$ in the above. These two steady solutions can now be used to construct the unsteady wake solution for $T \sim O(1)$, except in the region near $x \sim t$ or $X \sim T$.

2.2.3. *Unsteady wake solutions for* $T \sim O(1)$

We recall that for $T > 0$, $U = 1$ and introduce a change of variables $(X, T) \to (Y, S)$ defined by

$$Y = X, \quad S = T - X, \tag{35}$$

which results in $\partial/\partial T + \partial/\partial X = \partial/\partial Y$. Hence, (23)–(26) become

$$\hat{u}_Y + \hat{v}_R + \frac{1}{R}\hat{v} = 0, \tag{36}$$

$$\hat{u}_Y = \hat{u}_{RR} + \frac{1}{R}\hat{u}_R, \tag{37}$$

$$\hat{v}_Y = -\hat{p}_R + \hat{v}_{RR} + \frac{1}{R}\hat{v}_R - \frac{1}{R^2}\hat{v}, \tag{38}$$

$$\hat{\omega}_Y = \hat{\omega}_{RR} + \frac{1}{R}\hat{\omega}_R - \frac{1}{R^2}\hat{\omega}. \tag{39}$$

The boundary conditions are

$$\hat{u} = 0, \quad \hat{v} = 0, \quad \hat{p} = 0, \quad \text{and} \quad \hat{\omega} = 0 \quad \text{as} \quad Y \to \infty \quad \text{or} \quad R \to \infty. \tag{40}$$

These equations are identical to the steady wake equations with $U = 1$, and their solution is therefore given by (28)–(34) with $(X - X_0)$ replaced by $(Y - Y_0)$.

Physically, we expect that a new quasi-steady wake has formed behind the body in the region $0 < X < T$ while the old wake is swept away downstream of $X \sim T$. The transition zone between the new wake and the old wake is swept along with the flow at speed $U = 1$ as sketched in figure 1 (*a*). Hence, the solution for the new-wave velocity and stream function are simply

$$\hat{u}(X, R) = -\frac{\hat{Q}_2}{4\pi} \frac{1}{X - X_2} \exp\left[-\frac{R^2}{4(X - X_2)}\right] \quad \text{for} \quad 0 < X < T \tag{41a}$$

and

$$\hat{\psi}(X, R) = -\frac{\hat{Q}_2}{2\pi}\left\{1 - \exp\left[-\frac{R^2 U}{4(X - X_2)}\right]\right\} \quad \text{for} \quad 0 < X < T, \tag{41b}$$

where the subscript 2 denotes quantities corresponding to dimensional velocity U_2. The constant X_2 is the apparent origin of the new wake. The solution given by (41 *a*) satisfies (37) if we set $Y = X$ in (37).

The old wake was steady when the uniform upstream flow was $U = \alpha_{12}$; but the uniform flow has changed to $U = 1$. Hence, the old wake is swept downstream at dimensionless speed $(1 - \alpha_{12})$. We expect the steady solutions given by (28)–(34) to apply, with X replaced by $X - (1 - \alpha_{12})\, T$. In the coordinates moving with the body, $\hat{u}$ of the old wake is given by

$$\hat{u}(X, R) = -\frac{\hat{Q}_1}{4\pi} \frac{\alpha_{12}}{X - (1\text{-}\alpha_{12})\, T - X_1} \exp\left\{-\frac{\alpha_{12} R^2}{4[X - (1\text{-}\alpha_{12})\, T - X_1]}\right\}, \quad X > T. \tag{42a}$$

and

$$\hat{\psi}(X, R) = -\frac{\hat{Q}_1}{2\pi}\left\{1 - \exp\left[-\frac{\alpha_{12} R^2}{4(X - (1 - \alpha_{12})\, T - X_1)}\right]\right\}, \quad X > T. \tag{42b}$$

The solution for $\hat{u}$ is consistent with the unsteady solution

$$\hat{u}(S, Y, R) = -\frac{\hat{Q}}{4\pi} \frac{1}{Y - Y_0(S)} \exp\left\{-\frac{R^2}{4[Y - Y_0(S)]}\right\} \tag{43}$$

to (37) if we choose

$$\alpha_{12}[Y - Y_0(S)] = X - (1\text{-}\alpha_{12})\, T - X_1,$$

i.e.

$$Y_0(S) = \frac{1}{\alpha_{12}}[(1 - \alpha_{12})\, S + X_1] \tag{44}$$

and

$$\hat{Q} = \hat{Q}_1. \tag{45}$$

Hence, the unsteady (old) wake solutions are given by (42 *a*, *b*).

2.2.4. *Transition zone*

We need to join the new and old wake solutions near $X = T$; if we set

$$X = T - T_0 \tag{46}$$

we may determine T_0 from (41*a*) and (42*a*) which become

$$\hat{u} = -\frac{\hat{Q}_2}{4\pi}\frac{1}{T-T_0-X_2}\exp\left[-\frac{R^2}{4(T-T_0-X_2)}\right] \quad \text{(from new wake)} \tag{47a}$$

$$\hat{u} = -\frac{\hat{Q}_1}{4\pi}\frac{\alpha_{12}}{\alpha_{12}T-T_0-X_1}\exp\left[-\frac{R^2}{4(\alpha_{12}T-T_0-X_1)}\right] \quad \text{(from old wake).} \tag{47b}$$

We choose T_0 such that $\alpha_{12}(T_0+X_2) = T_0+X_1$, i.e.

$$T_0 = (\alpha_{12}X_2 - X_1)/(1-\alpha_{12}), \tag{48}$$

then denote $T_1 = X_2+T_0 = (X_2-X_1)/(1-\alpha_{12})$ to obtain

$$\hat{u} = -\frac{\hat{Q}_2}{4\pi}\frac{1}{T-T_1}\exp\left[-\frac{R^2}{4(T-T_1)}\right] \quad \text{(from new wake),} \tag{49a}$$

$$\hat{u} = -\frac{\hat{Q}_1}{4\pi}\frac{1}{T-T_1}\exp\left[-\frac{R^2}{4(T-T_1)}\right] \quad \text{(from old wake),} \tag{49b}$$

We are interested in the case with $\hat{Q}_1 \neq \hat{Q}_2$. Clearly, there is a discontinuity near $X \sim T$, or more precisely at $X = T-T_0$. This calls for a transition zone between these two wakes. The flow field in the transition zone may be resolved by including streamwise diffusion terms in the governing equations.

2.3. *Unsteady solutions in the transition zone*

2.3.1. *Re-scaling*

To understand the unsteady transition zone, the full equations (10)–(13) in the wake region must be reconsidered. Using a second re-scaling to resolve the transition zone,

$$X = T-T_0+\left(\frac{\epsilon}{Re'}\right)^{1/2}\xi, \tag{50}$$

$$\hat{v} = \left(\frac{Re'}{\epsilon}\right)^{1/2}V, \quad \hat{p} = \left(\frac{Re'}{\epsilon}\right)^{1/2}P, \tag{51a}$$

or

$$v = \epsilon V, \quad p = \epsilon^{3/2}Re'^{-1/2}P, \tag{51b}$$

and noting $\partial/\partial X \to (\epsilon/Re')^{-1/2}\partial/\partial\xi$, $\partial/\partial T \to \partial/\partial T-(\epsilon/R')^{-1/2}\partial/\partial\xi$, we obtain the following re-scaled equations:

$$\hat{u}_\xi + V_R + \frac{1}{R}V = 0, \tag{52}$$

$$\hat{u}_T + (\epsilon Re')^{1/2}(\hat{u}\hat{u}_\xi + V\hat{u}_R) = \hat{u}_{RR} + \frac{1}{R}\hat{u}_R + \hat{u}_{\xi\xi} - P_\xi, \tag{53}$$

$$V_T + (\epsilon Re')^{1/2}(\hat{u}V_\xi + VV_R) = V_{RR} + \frac{1}{R}V_R - \frac{1}{R^2}V + V_{\xi\xi} - P_R, \tag{54}$$

$$\hat{\omega}_T + (\epsilon Re')^{1/2}(\hat{u}\hat{\omega}_\xi + V\hat{\omega}_R) = \hat{\omega}_{RR} + \frac{1}{R}\hat{\omega}_R - \frac{1}{R^2}\hat{\omega} + \hat{\omega}_{\xi\xi}. \tag{55}$$

The boundary conditions and the matching conditions are

$$\hat{u},\quad V,\quad P \quad \text{and} \quad \hat{\omega}\to 0 \quad \text{as} \quad R\to\infty, \tag{56}$$

$$\hat{u} = -\hat{Q}_{1,2}\frac{1}{4\pi}\frac{1}{T-T_1}\exp(-\tfrac{1}{4}\eta^2) \quad \text{as} \quad \xi\to\pm\infty, \tag{57}$$

$$\hat{\omega} = -\hat{Q}_{1,2}\frac{1}{8\pi}\frac{\eta}{(T-T_1)^{3/2}}\exp(-\tfrac{1}{4}\eta^2) \quad \text{as} \quad \xi\to\pm\infty, \tag{58}$$

where

$$\eta = R/(T-T_1)^{1/2} \tag{59}$$

and $\hat{Q}_{1,2}$ denotes the respective upstream ($\hat{Q}_2$: $\xi\to-\infty$) and downstream ($\hat{Q}_1$: $\xi\to\infty$) values of $\hat{Q}$. We will first solve the leading-order problem for $\hat{\omega}$ from (55) and (58). The velocity component $\hat{u}$ can be obtained from

$$\frac{1}{R}(R\hat{u}_R)_R + \hat{u}_{\xi\xi} = -\frac{1}{R}(R\hat{\omega})_R \tag{60}$$

which results from the definition for $\hat{\omega}$ and mass conservation. The stream function $\hat{\psi}$ can be obtained by integrating $\eta\hat{u}$ with respect to η; the velocity component V can be obtained by differentiating $\hat{\psi}$.

At leading order, terms of $O((\epsilon Re')^{1/2})$ are dropped by requiring $\epsilon \ll Re'^{-1}$ or more directly $x \gg Re'$ and $t \gg Re'$ so that (53)–(55) can be simplified. The detailed procedure and the solutions for $\hat{\omega}$ (or $\zeta = R\hat{\omega}$), $\hat{u}$, and $\hat{\psi}$ in the transition zone are given in the Appendix.

The uniformly valid leading-order solution for the laminar far wake, $\hat{\psi}_{fw}$, can be easily constructed by uniformly joining the solutions in the new wake ($X < T-T_0$ or $\chi < 0$; see (A 12) for the definition of χ) given by (41*b*), in the old wake ($X > T-T_0$ or $\chi > 0$) given by (42*b*), and in the transition zone given by (A 23). Since $\hat{\psi}^{TZ}(\chi\to-\infty)$ and $\hat{\psi}^{TZ}(\chi\to+\infty)$ give the common parts on the left- and right-hand sides of the transition zone during matching, the far-wake solution for the stream function is

$$\hat{\psi}_{fw} = -\frac{\hat{Q}_2}{2\pi}\left\{1-\exp\left[-\frac{R^2U}{4(X-X_2)}\right]\right\} + \hat{\psi}^{TZ}(\chi,\eta) - \hat{\psi}^{TZ}(\chi\to-\infty), \quad \chi < 0 \tag{61a}$$

and

$$\hat{\psi}_{fw} = -\frac{\hat{Q}_1}{2\pi}\left\{1-\exp\left[-\frac{\alpha_{12}R^2}{4(X-(1-\alpha_{12})T-X_1)}\right]\right\} + \hat{\psi}^{TZ}(\chi,\eta) - \hat{\psi}^{TZ}(\chi\to+\infty), \quad \chi > 0. \tag{61b}$$

In the above, the subscript *fw* denotes far wake and superscript *TZ* denotes transition zone.

2.3.2. *Global consideration based on mass conservation*

To obtain a global description of the long-time unsteady flow induced by the sudden change in the velocity of the body, we consider a spherical control volume C_v centred on the body with a radius much larger than t that contains the entire new wake, the transition zone, and a part of the old wake. Mass conservation in C_v requires that the flux entering the old wake and the sink in the transition zone be balanced by the source

near the origin $x = 0$. Although the contribution to the wake velocity from the source is of $O(x^{-2})$ and smaller than the $O(x^{-1})$ velocities of the old and new wakes, this source is physically important to ensure the overall mass balance. Hence, for a physically realistic description of the flow, the solution for the stream function for the entire flow field must include the following contribution from the source near $x = 0$:

$$\hat{\psi}_s = \frac{1}{4\pi}\hat{Q}_2\left\{1 - \frac{x - x_2}{[(x-x_s)^2 + r^2]^{1/2}}\right\}, \tag{62}$$

where x_s is the location of the source. The entire flow field can now be analytically constructed using $\hat{\psi}_s$ and the unsteady far-wake solution $\hat{\psi}_{fw}$ as follows:

$$\hat{\psi} = \begin{cases} \hat{\psi}_{fw} + \hat{\psi}_s & \text{for} \quad x > 0 \\ \hat{\psi}_{TZ,S} + \hat{\psi}_s - \dfrac{\hat{Q}_1}{2\pi} & \text{for} \quad x < 0, \end{cases} \tag{63}$$

where $-\hat{Q}_1/2\pi$ accounts for the contribution of the old wake to $\hat{\psi}$ in the upstream region and ensures that $\hat{\psi}(r = 0,\ x < 0) = 0$, and

$$\hat{\psi}_{TZ,S} = \frac{1}{4\pi}(\hat{Q}_1 - \hat{Q}_2)\left\{1 - \frac{x - t + t_0}{[(x-t+t_0)^2 + r^2]^{1/2}}\right\} \tag{64}$$

is the stream function of the sink (or source if $Re_1 > Re_2$) at the transition zone whose contribution to the region of $x > 0$ has been effectively included in ψ_{fw} by (61). For $x < 0$, the wake solution ceases to apply while the effect of the sink at the small transition zone represented by (64) is valid outside the transition zone.

The corresponding contribution of the source near $x = 0$ to the velocity field is

$$\hat{u}_s = \frac{1}{4\pi}\hat{Q}_2\frac{x - x_s}{[(x-x_s)^2 + r^2]^{3/2}}, \quad \hat{v}_s = \frac{1}{4\pi}\hat{Q}_2\frac{r}{[(x-x_s)^2 + r^2]^{3/2}}. \tag{65}$$

Since the source flow is irrotational, its contribution to the vorticity is zero.

2.4. *Unsteady flow due to impulsive stop of the body*

Consider a body moving at a speed $U_1 = 1$ from left to right. When it is suddenly brought to rest, the wake behind the body will continue to move to the right with the wake origin travelling as $x \sim t$. The source associated with the body will, however, stop at $x = x_s$ near the origin. Since the body at rest does not supply any momentum to the surroundings, the flow due to the source will diffuse out and the region around $x = x_s$ serves as a transition zone to connect the travelling old wake and the source flow.

The wake velocity and vorticity on the left of the body is given by (cf. (42))

$$\hat{u} = \frac{\hat{Q}_1}{4\pi}\frac{1}{T - X - X_1}\exp\left[-\frac{R^2}{4(T - X - X_1)}\right], \quad X < 0, \tag{66}$$

$$\hat{\omega} = \frac{\hat{Q}_1}{8\pi}\frac{R}{(T - X - X_1)^2}\exp\left[-\frac{R^2}{4(T - X - X_1)}\right], \quad X < 0, \tag{67}$$

$$\hat{\psi} = \frac{\hat{Q}_1}{2\pi}\left\{1 - \exp\left[-\frac{R^2}{4(T - X - X_1)}\right]\right\}, \quad X < 0, \tag{68}$$

where X_1 is the apparent origin of the old wake relative to the sphere for $T < 0$. In the transition zone, $X = X_s \ll 1$, the above become

$$\hat{u} = \hat{Q}_1 \frac{1}{4\pi} \frac{1}{T - T_1} \exp(-\tfrac{1}{4}\eta^2), \tag{69}$$

$$\hat{\omega} = \hat{Q}_1 \frac{1}{8\pi} \frac{\eta}{(T - T_1)^{3/2}} \exp(-\tfrac{1}{4}\eta^2), \tag{70}$$

$$\hat{\psi} = \frac{\hat{Q}_1}{2\pi} [1 - \exp(-\tfrac{1}{4}\eta^2)], \tag{71}$$

where $T_1 = X_1 + X_s$ and $\eta = R/(T - T_1)^{1/2}$. On the right of the transition zone, $X > 0$, we have

$$\hat{\omega} = 0. \tag{72}$$

Using

$$X = X_s + \left(\frac{\epsilon}{Re'}\right)^{1/2} \xi \tag{73}$$

in lieu of (50) to rescale X, noticing that $U = 0$ in (18)–(21) in the impulsive stop case, we again obtain (52)–(55). Using the matching conditions (69)–(72), we found

$$\hat{\omega} = \hat{Q}_1 \frac{1}{16\pi} \frac{R}{(T - T_1)^2} \exp\left[-\frac{R^2}{4(T - T_1)}\right] \operatorname{erfc}(\tfrac{1}{2}\chi) \tag{74}$$

which integrates to

$$\hat{u} = \hat{Q}_1 \frac{1}{4\pi(T - T_1)} \left\{ \tfrac{1}{2} \operatorname{erfc}(\tfrac{1}{2}\chi) \exp(-\tfrac{1}{4}\eta^2) + \cos\theta \left[\frac{1}{\sigma^2} \operatorname{erf}(\tfrac{1}{2}\sigma) - \frac{1}{\sigma \pi^{1/2}} \exp(-\tfrac{1}{4}\sigma^2) \right] \right\} \tag{75}$$

and

$$\hat{\psi}^{TZ} = \frac{1}{4\pi} \hat{Q}_1 [1 - \exp(-\tfrac{1}{4}\eta^2)] \operatorname{erfc}(\tfrac{1}{2}\chi) + \frac{1}{4\pi} \hat{Q}_1 [\operatorname{erf}(\tfrac{1}{2}\chi) - \cos\theta \operatorname{erf}(\tfrac{1}{2}\sigma)]. \tag{76}$$

For $\sigma \to \infty$ and $\chi > 0$ we have $\hat{u} \to \hat{Q}_1 \cos\theta / [4\pi(T - T_1)] (1/\sigma^2)$ which describes a source flow. Since $\hat{\psi}^{TZ}(\chi \to -\infty) = (\hat{Q}_1/2\pi)[1 - \exp(-\tfrac{1}{4}\eta^2)]$ gives the common part on the left-hand side of the transition zone during matching with the wake solution given by (71), the uniformly valid far-field solution, $\hat{\psi}$, is

$$\hat{\psi} = \frac{\hat{Q}_1}{2\pi} \left\{ 1 - \exp\left[-\frac{R^2}{4(T - X - X_1)} \right] \right\} + \hat{\psi}^{TZ}(\chi, \eta) - \frac{\hat{Q}_1}{2\pi} [1 - \exp(-\tfrac{1}{4}\eta^2)], \quad \chi < 0 \tag{77a}$$

and

$$\hat{\psi} = \hat{\psi}^{TZ} \quad \chi > 0. \tag{77b}$$

A comparison of the asymptotic solution and the finite difference solution of the large-scale flow field will be presented in §3.

2.5. *Unsteady flow due to an impulsive reverse of the body*, $\alpha_{12} < 0$

Consideration is now given to the body moving from left to right at a speed $|\alpha_{12}|$ for $t < 0$. There is an old wake of volume flux $\hat{Q}_1$ on the left-hand side of the body and the wake is moving to the right. When the object is suddenly reversed, it encounters the old

wake on the left. For the purpose of understanding the global flow field, the reversing process of the body can be conveniently split into two stages without affecting the long-time asymptotic feature of the flow: (*a*) the body suddenly stops at $t = 0^-$; and (*b*) the body then suddenly moves to the left at $t = 0^+$ with a speed 1. The basic elements of the flow field associated with these two impulsive processes have been discussed in detail in §§2.3 and 2.4. After the stop, a source of volume flux $\hat{Q}_1$ at time t is located at $x \sim t$ relative to the moving body and diffuses out radially. After the impulsive start, there is a new wake with a volume flux $\hat{Q}_2$ moving to the left in $0 < x < t$ and a sink of volume flux $\hat{Q}_2$ located at $x \sim t$. Thus, there is an equivalent net sink of volume flux $(\hat{Q}_2 - \hat{Q}_1)$ at $x \sim t$. There is also a source of volume flux $\hat{Q}_2$ attached to the body at $x \sim 0$. The flow in the upstream region due to the source $\hat{Q}_2$ then encounters the old wake that is moving to the right at speed $|\alpha_{12}|$ relative to a fixed reference frame with the apparent origin at $x \sim (1-\alpha_{12})t$. These principal features of the flow due to the impulsive reverse of the body are shown in figure 1(*b*). Pedley (1975) studied the response of a thermal boundary layer over a finite-length plate to a spatially uniform but temporally reversing flow near $t = 0$. There is a certain similarity in the nature of the long-time behaviour of the thermal boundary layer in Pedley's work and the far-wake velocity field in the present case. During the flow reversal, the short-time behaviour in the near field is dominated by the diffusion which depends strongly on the geometry of the problem and the behaviour of the acceleration.

Some quantitative estimations of the interaction between the old wakes and a moving sphere can be readily obtained. It is noted that for a sphere moving to the left at finite Reynolds number, the global flow at a large r should be dictated by the source–wake combination (Batchelor 1967, p. 351) and the upstream velocity is thus, at large $|x|$,

$$u_{up}(x) = u_{up}^{source}(x) = -\frac{3\phi_2}{Re}\frac{1}{x^2}, \tag{78a}$$

where (29*a*, *b*) are used for the source volume flux associated with the sphere. If Re_2 is very small, creeping flow is a valid representation of the actual flow within some distance from the sphere; and the upstream ($x < 0$) velocity is then

$$u_{up}(x) = u_{up}^{creeping}(x) = \frac{1}{2}\left(\frac{3}{x} - \frac{1}{x^3}\right). \tag{78b}$$

At very large distance, $u_{up}^{source}(x)$ takes over because the creeping flow solution is no longer valid and the source–wake combination is again the dominating feature. We can also use the steady-state finite difference (FD) solution, $u_{up}^{FD}(x)$, to represent the actual upstream velocity at a given Re; this is especially useful since we do not know the exact regions of validity of the various forms of $u_{up}(x)$ given by (78).

After the sphere reverses, the velocity due to the old wake at $x < 0$ is

$$u_{wake}(x) \sim \frac{3\phi_1}{2}\frac{|\alpha_{12}|}{(1-\alpha_{12})t - x} \tag{79}$$

to the leading order. When the flow described by $u_{up}(x)$ is superposed on this old wake, the upstream centreline velocity can be estimated as

$$u(x) \sim u_{up}(x, Re_2) + \frac{3\phi_1}{2}\frac{|\alpha_{12}|}{(1-\alpha_{12})t - x} \quad \text{for} \quad x < 0. \tag{80}$$

The upstream stagnation point, x_{up}, can thus be predicted by setting $u(x) = 0$ in the above. To the leading order, (78*a*, *b*) give

$$x_{up}^{source} \sim -\left[\frac{2(1-\alpha_{12})\,\phi_2\,t}{Re_2|\alpha_{12}|\,\phi_1}\right]^{1/2}, \quad x_{up}^{creeping} \sim -\frac{(1-\alpha_{12})\,t}{|\alpha_{12}|\,\phi_1}. \tag{81a, b}$$

In the above, x_{up}^{source} is valid if x_{up} is large, say for extremely large t. It is interesting to note that the stagnation point for very small Re_2 moves to the left with nearly constant speed for some finite time; eventually it slows down with $x_{up} \sim t^{1/2}$. For finite Re_2 the motion of the upstream stagnation point is $x_{up} \sim t^{1/2}$ except for very small t for which (79) may not be valid.

In the downstream region, the flow field is complicated by the diffusing source near $x \sim t$. However, when $Re_1 = Re_2$, the strength of the diffusing source is equal to that of the sink in the transition zone; hence their effects are nearly cancelled locally. The downstream flow is thus dictated by the new wake and the old wake. For $\alpha_{12} = -1$, the downstream stagnation point x_{down} is $x_{down} \sim t + x_2$ to the leading order where x_2 is the artificial origin of the new wake relative to the sphere. Thus the separation point stays near the location where the sphere reverses.

To recapitulate, the long-time global flow field due to the impulsive reversal of the body has the following principal elements that may serve as building blocks for understanding more complex flows. (*a*) There is an old wake with its origin moving at $x \sim (1-\alpha_{12})\,t$. The velocity of this old wake is valid for $x < t$ but far away from the body. (*b*) There is a diffusing source at $x \sim t$ with a volume flux $(\hat{Q}_1 - \hat{Q}_2)$. (*c*) There is a new source of volume flux $\hat{Q}_2$ at $x \sim 0$ and a new wake in $0 < x < t$.

3. Finite difference solution

The foregoing asymptotic analyses for velocity, vorticity and stream function and the results presented in LM clearly show that the unsteady wake, including the small transition zone, must be resolved to sufficiently capture the strength of the sink and therefore the transient force. In an earlier computational work (Mei 1993) no particular attention was paid to the resolution in the transition zone; hence the transient force was inaccurate at very large time. In fact a slow exponential decay was observed for the step change case ($U_2 U_1 > 0$) for all Reynolds numbers as long as the computation lasted sufficiently long. The exponential decay is now known to be incorrect (LM). Hence a different gridding strategy must be adopted.

Because we are interested in the long-time ($t \gg 1$) behaviour of the flow field and the drag, and the transition zone is located at $x \sim t \gg 1$, it is computationally very demanding to resolve simultaneously the flow field near the sphere on which the vorticity is created and the flow field within the transition zone which determines the transient force. Using spherical coordinates (r, θ) centred on the sphere with $\theta = \pi$ lying on the centreline of the wake, the equations governing the vorticity and the stream function and the boundary conditions are exactly as given in Mei (1993) and details are given in that reference. To achieve a better resolution in the transverse direction of the wake, the governing equations are written in transformed coordinates (ξ_1, ξ_2). A non-uniform stretching in the θ-direction is introduced:

$$\theta = \pi c_\theta \tan^{-1}[\xi_1 \tan(1/c_\theta)], \quad 0 \leqslant \xi_1 \leqslant 1. \tag{82}$$

With $c_\theta = 0.8$, the grid spacing $\Delta\theta$ at $\theta = \pi$ is only one tenth of $\Delta\theta$ at $\theta = 0$. For the impulsive stop and reverse, no stretching in the θ-direction is necessary because the t^{-1}

behaviour of the transient force is established much earlier than the t^{-2} behaviour; and $t \sim 50$–75 is sufficient. For the steady-state results given in figure 2(*b*) for the upstream velocity, the stretching in the θ-direction is not applied. A very large value of c_θ is taken to obtain a uniform grid. In the r-direction, the same stretching as used in Mei (1993) is employed; no particular stretching is applied near the moving transition zone at $x \sim t$. Hence,

$$r = 1+(r_E-1)\{1-c_r \tan^{-1}[(1-\xi_2)\tan(1/c_r)]\}, \quad 0 \leqslant \xi_2 \leqslant 1, \tag{83}$$

in which r_E is the size of the spherical domain. The numerical computation is performed using $n_r = 257$ grid points in the r-direction, $n_\theta = 129$ grid points in the θ-direction, $c_r = 0.645$, $c_\theta = 0.8$, and $r_E = 1200$. With this arrangement, it turns out that the resolution is usually sufficient for $t < 300$ with a t^{-2} decay for the transient force; beyond $t \sim 300$, the resolution in the transition zone at $x \sim t$ is lost and the strength of the sink is reduced, possibly due to numerical diffusion associated with large Δr at $r \sim 300$, which results in a decay faster than t^{-2} for the transient force. Fortunately, $t \sim 300$ is sufficient to capture the long-time asymptotic features of the unsteady flow, field, as shown in LM.

The computation is carried out in transformed coordinates (ξ_1, ξ_2). The second-order spatial derivatives are expressed using central difference. The convection term is discretized using a second-order upwind scheme in a conservative form (Mei & Plotkin 1986) in both directions. The time derivative is evaluated using a backward Euler scheme which is implicit and first-order accurate in time. The numerical boundary condition for the vorticity is evaluated from the stream function on the grid points near the wall using a second-order-accurate expression. Double precision is used for all computations. The rest of the computational details can be found in Mei (1993). After the uniform flow over a stationary sphere is obtained, it is subtracted to yield the unsteady flow induced by a moving sphere. The Reynolds number of the flow, Re, is defined based on the diameter, $Re = 2aU/\nu$.

4. Comparison of finite difference and asymptotic results

To verify the accuracy of the numerical solution for flow over the sphere in a large spatial region, the steady-state wake velocity obtained from the present computation using the refined and stretched grids is compared with the steady wake velocity from the analytical solution. It is noted that at steady state the present asymptotic solution for the wake velocity is identical to that of Batchelor (1967). Because the asymptotic wake solution is valid only in the far wake, there is some arbitrariness in the apparent origin, x_0, of the wake. By taking the source contribution (see (78*a*)) into account to maintain the global mass balance, the centreline wake velocity can be expressed as

$$u(x) \sim -\frac{\frac{3}{2}\phi}{x-x_0}+\frac{3\phi/Re}{(x-x_s)^2}. \tag{84}$$

The apparent origin may be chosen by requiring no-slip conditions at $x = 1$, i.e. $u(x = 1) = -1$). Hence

$$x_0 = 1-\frac{3\phi Re(1-x_s)^2}{2Re(1-x_s)^2+6\phi}. \tag{85}$$

It is noted that the contribution due to the source can be made ineffective by taking a large $-x_s$; in this case $x_0 = 1-\frac{3}{2}\phi$. Because the near-wake solution is not pursued in the present analysis, the apparent origin x_0 of the wake can be used simply as a 'free'

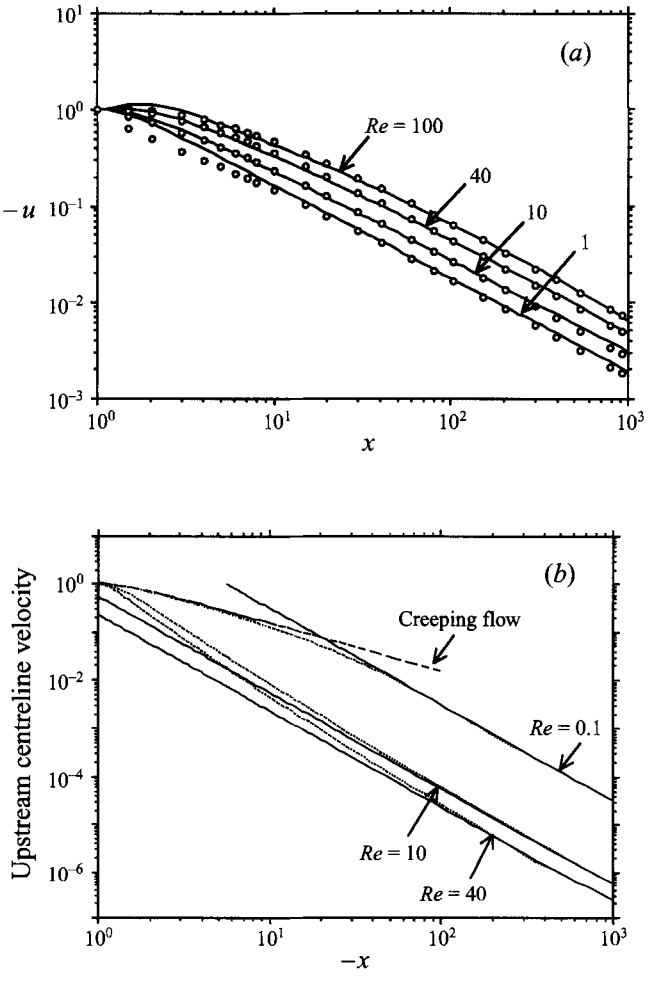

FIGURE 2. (*a*) Comparison of the numerical solution and asymptotic solution for the steady wake centreline velocity for $Re = 1$, 10, 40 and 100. Open circles: finite difference solutions; solid lines: analytical approximation. (*b*) Comparison of various solutions for the upstram centreline velocity at steady state for $Re = 0.1$, 10 and 40. Solid lines: u_{up}^{source}; dashed lines: $u_{up}^{creeping}$; dotted lines: finite difference solutions.

parameter to adjust the analytical solution so that good agreement between the theory and the numerical solution can be obtained in the near-wake region. In general, it is appropriate to obtain x_0 and x_s from the steady-state numerical solution.

Figure 2(*a*) shows the steady wake centreline velocities obtained from the numerical solution and the analytical approximation given by (84) for $Re = 1$, 10, 40, and 100. From trial and error, it is found that the following artificial origins result in good fits for each $u(x; Re)$: $x_s = -0.99$, -0.9, 0, and 0.2 for $Re = 1$, 10, 40 and 100. There is slight disagreement between the finite difference and the asymptotic wake solutions near $x = o(1)$ for $Re = 1$. This is entirely caused by our limiting x_s to be within the sphere. If a large $-x_s$ is used, a much better agreement can be obtained for the $Re = 1$ case. When the global flow field is considered (see (62)–(63)), however, such a source outside the sphere is not preferred. Hence, $|x_s| < 1$ is imposed. A few diameters away from the sphere, excellent agreement is observed for u over two to three decades of x

for all four cases. Thus these values for x_s can be used in describing the velocity and stream function of the unsteady flow. It is noted that if the stretching in the θ-direction is not applied, the wake velocity would decay exponentially at very large x for $Re = 40$ and 100, in an otherwise identical grid system, owing to insufficient resolution in the transverse direction in the wake at large distance; see (31) for the exponent. Hence the stretching in the θ-direction is necessary in numerous cases considered here.

Figure 2(*b*) compares the upstream centreline velocity based on the finite difference solutions at $Re = 0.1$, 10 and 40 with the corresponding $u_{up}^{creeping}$, and u_{up}^{source}. For $Re = 0.1$, 10 and 40, $r^2 u_{up}^{source} = 30.474$, 0.5378, and 0.2240, respectively, as shown by the solid lines. The case $Re = 0.1$ can be considered as in the low-Re regime. It is seen that the exact u_{up} given by the finite difference solution can be represented quite well by $u_{up}^{creeping}$ for $r < 10$. For $r > 40$, u_{up}^{source} takes over. For $Re = 10$, u_{up}^{FD} can be roughly approximated by u_{up}^{source} for $r > 80$. For $Re = 40$, u_{up}^{source} represents u_{up}^{FD} well for $r > 100$. The behaviour of u_{up} is important in analysing the flow field due to an impulsive reversal of the sphere. The comparisons shown in figure 2 suggest that the present finite difference solutions are accurate and agree well with known asymptotic limits in both the upstream and downstream directions.

In approximating the wake velocity, the choice of x_0 is critical to the good agreement in the region $x \sim 10$ between the analytical and numerical predictions for the wake velocity. As seen from (85), x_0 is strongly influenced by x_s. It is noted that the source at $x = x_s$ does not affect the vorticity field. When the wake vorticity is considered, it is natural that x_0 for the vorticity would be different in order to achieve a good fit with the numerical solution. Physically, different values of x_0 are taken because the structures for the velocity and vorticity in the near wake are not the same.

For the unsteady flow, the choice of x_2 (the origin of the new wake) is somewhat more important than that of x_1 (the origin of the old wake) because the old wake is already far downstream. In the asymptotic solution, t_0 determines the exact location of the transition zone, $x = t - t_0$; but t_0 is left undetermined in the leading-order asymptotic solution. Physically the transition zone is associated with the sink. Hence, t_0 for the velocity, vorticity, and stream function should be the same. In the detailed comparisons to follow between the asymptotic and finite difference solutions, we shall determine t_0 based on the best agreement of the basic flow structures between the two solutions. Once t_0 and x_2 are specified, x_1 is found from (48) as $x_1 = \alpha_{12} x_2 - (1 - \alpha_{12}) t_0$ and $t_1 = x_2 + t_0$. The asymptotic solutions are less sensitive to (x_1, t_1) than to (x_2, t_0). It is emphasized that the relation between x_1, x_2 and t_0 given by (48) must be satisfied for a smooth velocity in the transition zone.

Figure 3(*a*) compares the asymptotic and numerical solutions for the unsteady wake centreline velocity $u(x)$ for the impulsive-start case with $Re_2 = 1$ and $Re_2 = 40$ at $t = 40$. For $Re_2 = 1$, we choose $t_0 = 0$, $x_2 = 0$ for the vorticity, and $x_s = -0.99$ to give $x_2 = 0.084$ for $u(x)$. For $Re_2 = 40$, $t_0 = 2.5$, $x_2 = -5.5$ for the vorticity, and $x_s = 0$ so that $x_2 = -2.66$ for the velocity. The agreement for the centreline velocity in the new-wake region ($x < t - t_0$) is excellent. The agreement in the transition zone at $x \sim t - t_0$ is also very good for $Re_2 = 1$. For $Re_2 = 40$ the asymptotic structure of the transition zone is well predicted and the agreement is considered good. For $x > t - t_0$, there is no old wake and the flow is dictated by the sink at the transition zone and the source at $x \sim 0$. For $x \gg t$, the velocity behaves as $(\hat{Q}_2 t/2\pi)(x - t/2)^{-3}$ which results from the source at $x \sim 0$ and the sink at $x \sim t - t_0$. The agreement between the asymptotic and numerical solutions is excellent for such small values of $u(x)$ over a large range of x.

It is worth noting that the asymptotic analyses for the far wake described in the previous sections are also applicable to flow over bubbles. The major difference

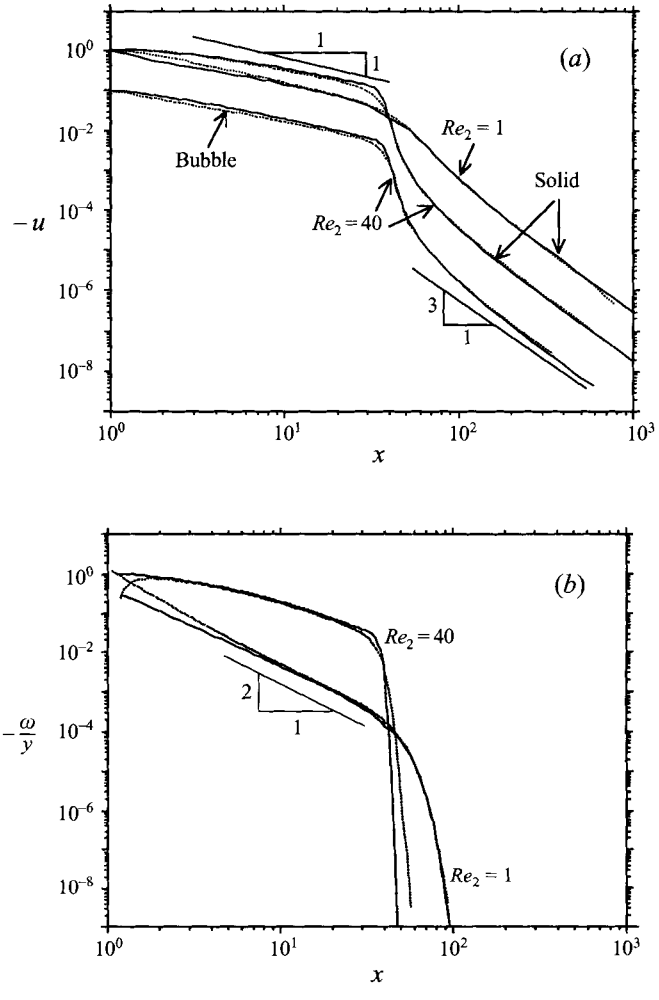

FIGURE 3. (*a*) Comparison of the numerical solution (dotted lines) and matched asymptotic expansion (solid lines) for the wake centreline velocity for the impulsively started motion of solid sphere ($Re_2 = 1$ and 40) and spherical bubble ($Re_2 = 40$) at $t = 40$. The curve for the bubble has been shifted downward by one decade for clarity. (*b*) As (*a*) but comparing the wake off-centreline vorticity ($\pi - \theta = 0.00592$).

between a solid sphere and a clean bubble is that the shear stress on the bubble surface is zero. Thus the flow near the bubble, including the near-wake region, is quite different from the solid-sphere case. However, in the far-wake region, since the governing mechanism for the vorticity transport is identical, it is expected that the forgoing analyses are also valid for flow over the bubble. Figure 3(*a*) also shows a comparison of the centreline velocity behind the bubble for the impulsive-start case with $Re_2 = 40$. The agreement between the asymptotic analyses ($t_0 = 1$, $x_s = 0$; $x_2 - 0.85$) and the finite difference results is as good as for the solid-sphere case. The magnitude of the history force on the bubble was addressed in Mei, Klausner & Lawrence (1994). The transient force on the bubble in the impulsive-start case at $Re = 40$ was reported also in LM and good agreement between finite difference computation and the asymptotic analysis for the transient force was obtained.

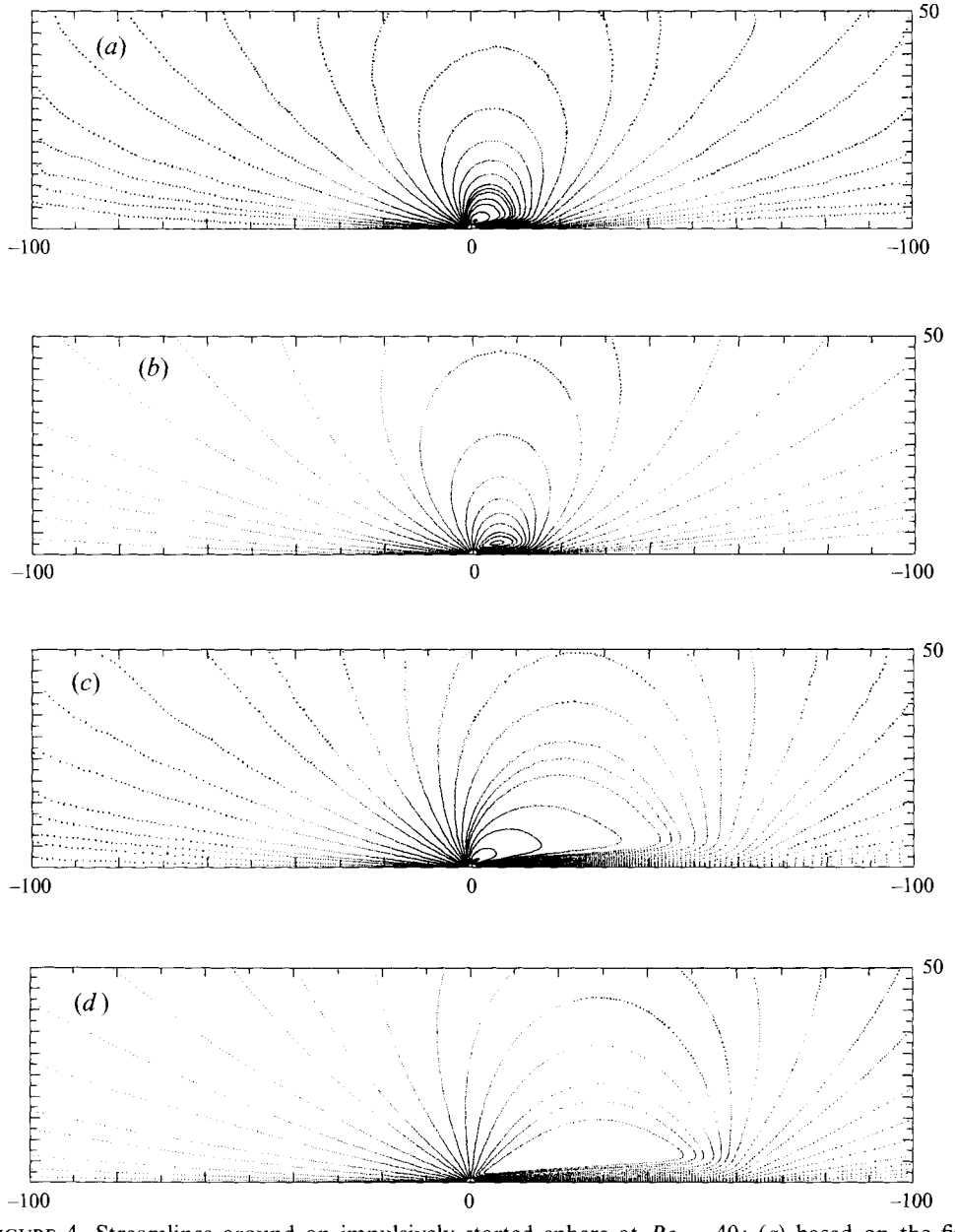

FIGURE 4. Streamlines around an impulsively started sphere at $Re_2 = 40$: (*a*) based on the finite difference solution at $t = 15$; (*b*) asymptotic solution at $t = 15$; (*c*) based on the finite difference solution at $t = 60$; (*d*) asymptotic solution at $t = 60$.

Since the vorticity ω is identically zero on the centreline of the wake, $\theta = \pi$, we choose to compare the asymptotic and the numerical solutions for ω/y ($y \equiv r\sin\theta$) on the first grid line off the wake centreline. Hereinafter (r, θ) denote the spherical coordinates centred on the sphere. Figure 3(*b*) compares the asymptotic and numerical solutions for ω/y on the first grid off the wake centreline ($\pi - \theta = 0.00592$) for the impulsive-start case with $Re_2 = 1$ and $Re_2 = 40$ at $t = 40$. The agreement between the two solutions is excellent for the new wake at $x < t$. The decay of ω/y in the transition zone is well predicted for $Re_2 = 1$. For $Re_2 = 40$, the qualitative agreement, i.e. the

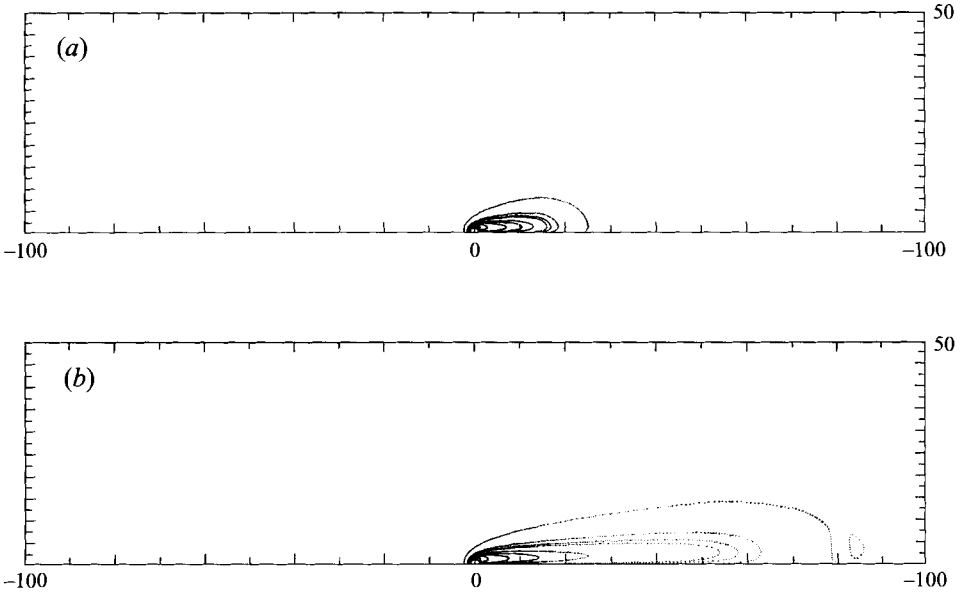

FIGURE 5. Vorticity contours of the flow field around an impulsively started sphere at $Re_2 = 40$ based on the finite difference solution. (*a*) $t = 15$; (*b*) $t = 60$.

rapid decay of ω/y in the transition zone is predicted by both solutions. The slightly slower decay of the numerical solution may result from the leakage of the vorticity through extra numerical diffusion associated with finite grid size and time-step size. This extra numerical diffusion is also present when $Re_2 = 1$ on the same grid, but the physical diffusion appears to dominate. For $Re_2 = 40$, the physical diffusion is quite small and the extra numerical diffusion smears out the transition zone and transports vorticity further downstream.

Figure 4(*a–d*) shows the streamlines due to an impulsively started sphere with $Re_2 = 40$ at $t = 15$ and $t = 60$ based on the finite difference solution and the analytical approximation given by (63). Bearing in mind that the asymptotic solution formally requires $t \gg Re'$, the agreement between the two solutions is remarkably good. The large-scale flow field around the sphere at $t = 15$ is basically a pair of source and sink induced by the impulsive start of the sphere. Close examination also indicates that the pair is stretched with the sink located at $x \sim t = 15$. As t increases, the flow field evolves and the pair is clearly split into a source attached to the sphere and a sink at $x \sim t$ moving to the right. As seen from figure 4(*c*, *d*) for $t = 60$, a quasi-steady wake is clearly established between $x = 0$ and $x \sim t$. When the steady state is reached, the sink has moved to infinity and the flow field surrounding the sphere in practice consists of the source (split from the pair) and a wake. Comparing figure 4(*a*) with 4(*b*), it is seen that even for $t = 15 < Re_2/2$ the flow field within the wake and the flow induced by the sink are well predicted by the asymptotic solution.

Figure 5(*a*, *b*) shows the vorticity contours of the flow field around an impulsively started sphere with $Re_2 = 40$ based on the finite difference solution at $t = 15$ and 60. While the region of influence on the flow field of the source–sink pair extends far beyond $x \sim t$, the vorticity is confined in the new wake, $x < t$, since the pair is irrotational. The new wake can also be viewed as acting as a 'vortex pipe'. Fluid is pulled in at the transition zone, carried along inside the wake and ejected near the body. This flow is both confined and maintained by the vorticity of the wake.

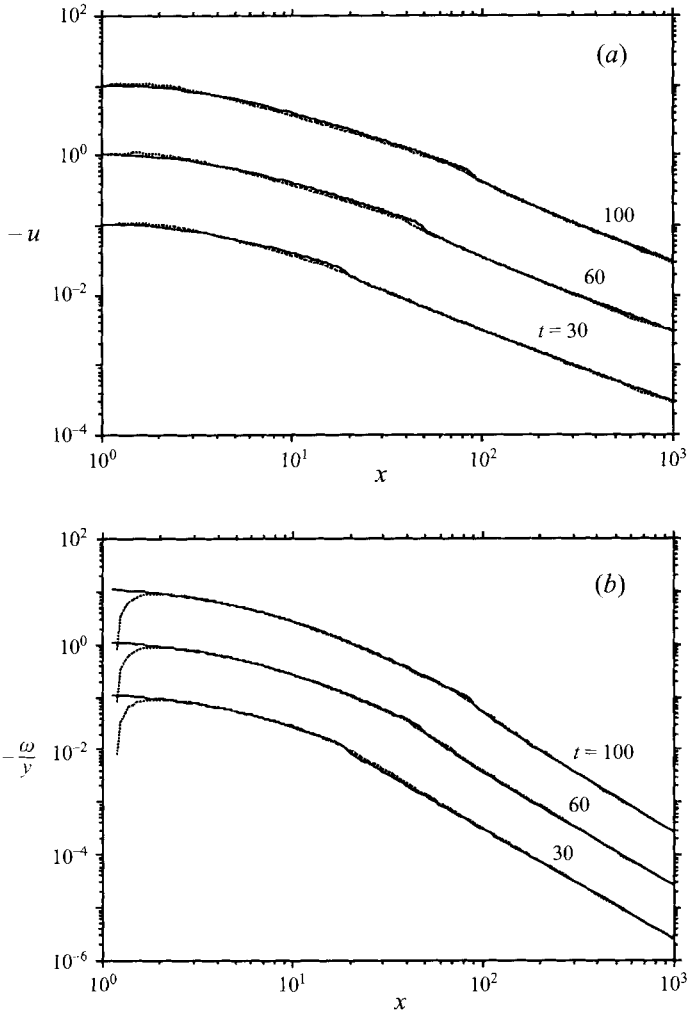

FIGURE 6. (*a*) Comparison of the numerical solution (dotted lines) and matched asymptotic expansion (solid lines) for the wake centreline velocity for sudden increase in the velocity from $Re_1 = 40$ to $Re_2 = 60$ at $t = 30$, $t = 60$ and $t = 100$. The curves for $t = 30$ and $t = 100$ have been shifted downward and upward by one decade respectively. (*b*) As (*a*) but comparing the wake off-centerline vorticity ($\pi - \theta = 0.00592$).

Figure 6(*a*) shows the unsteady wake centreline velocity $u(x)$ for a sudden change in the sphere velocity from $Re_1 = 40$ to $Re_2 = 60$ at $t = 30$, 60 and 100. We choose $t_0 = 11.5$, $x_2 = -3.54$ for $u(x)$ and $x_2 = -7.5$ for ω/y. The movement of the transition zone near $x \sim t$ relative to the sphere can be clearly observed. The agreement for $u(x)$ is good for both new and old wakes. Without the guidance of the analytical solution, it was difficult to discern the transition zone from the numerical solution. The analytical solution is thus quite useful in revealing the asymptotic structure of the unsteady wake. Figure 6(*b*) shows the off-centreline vorticity, ω/y, at $\pi - \theta = 0.00592$ based on the two solutions for the same case at $t = 30$, 60 and 100. Excellent agreement is observed. It is noted that at $x \sim t = 30$, the conditions $x \gg Re' = Re_2/2 = 30$, $t \gg Re' = 30$, which are necessary for obtaining the asymptotic solution in the transition zone, are not satisfied; yet the agreement between the asymptotic and numerical solutions in both

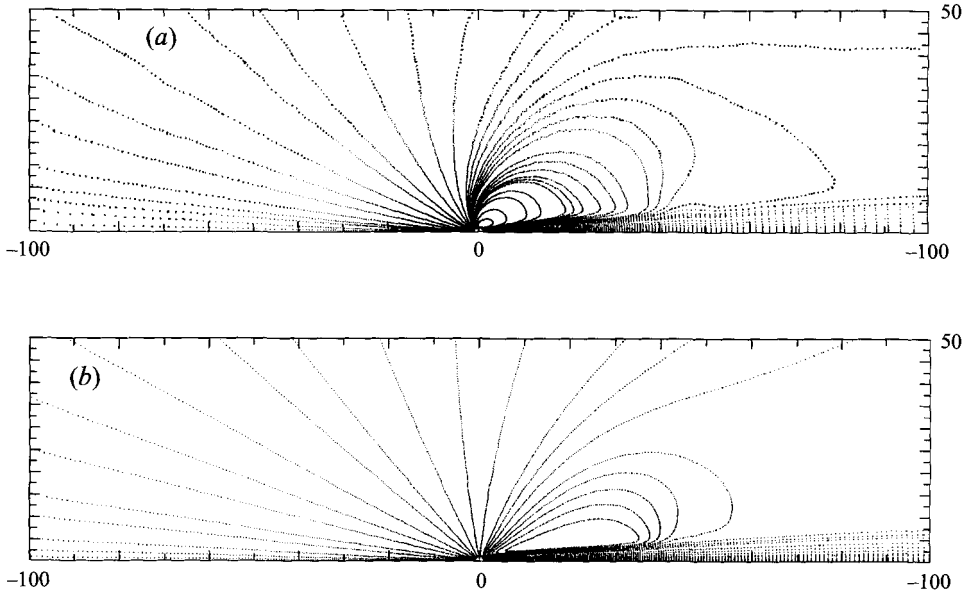

FIGURE 7. Streamlines around a sphere with a sudden increase in the velocity from $Re_1 = 40$ to $Re_2 = 60$ at $t = 50$: (*a*) based on the finite difference solution; (*b*) analytical approximation.

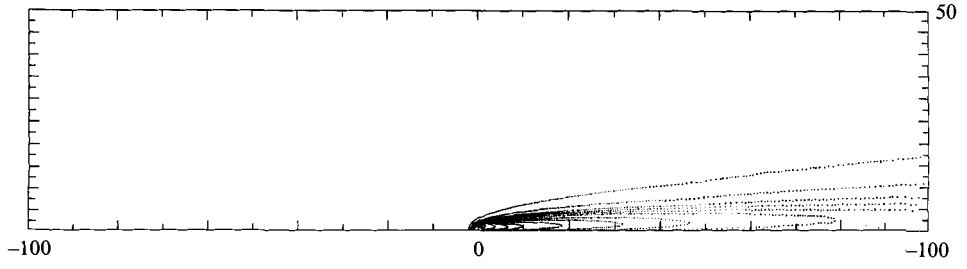

FIGURE 8. Vorticity contours of the flow field around a sphere with a sudden increase in the velocity from $Re_1 = 40$ to $Re_2 = 60$ based on the finite difference solution at $t = 50$.

cases is quite satisfactory. The agreement is even better for the case with $(Re_1, Re_2) = (10, 15)$ at $t = 30$, 60 and 100 (not shown here) with the choice of $t_0 = 6$, $x_2 \approx -1.34$ for $u(x)$ and $x_2 = -3.5$ for ω/y.

Figure 7(*a*, *b*) shows the streamlines for the case with a sudden change in velocity from $Re_1 = 40$ to $Re_2 = 60$ at $t = 50$ based on the numerical and asymptotic solutions. The sink is much weaker than for the impulsive start. As shown in LM, for small Re, the strength of the sink is of $O(Re^2)$ for a sudden change while it is of $O(Re)$ for the impulsive start. The sink at $x \sim t = 50$ is difficult to discern from the numerical solution; this is consistent with the observation for the wake centreline velocity $u(x)$ in which the transition zone was difficult to identify from the numerical solution at first glance. However, in figure 7(*b*), the asymptotic solution clearly shows that the flow field in the far-wake region, $x \gg 1$, consists of a new wake at $x < t$, an old wake at $x > t$, and a sink near $x \sim t$. Figure 8 shows the vorticity contours of the flow field around the sphere with a sudden increase in the velocity from $Re_1 = 40$ to $Re_2 = 60$ based on the finite difference solution at $t = 50$. The change of the slope in the contour lines at $x \sim t$ is visible; the vorticity contours near $x \sim t$ exhibit concave behaviour.

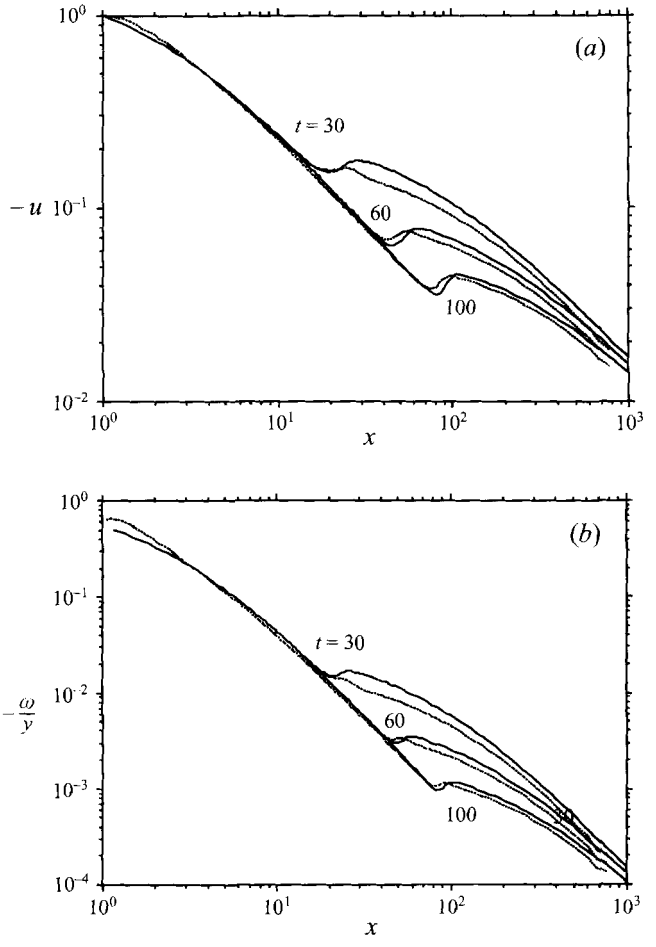

FIGURE 9. (*a*) Comparison of the numerical solution (dotted lines) and matched asymptotic expansion (solid lines) for the wake centreline velocity for a sudden decrease in the velocity from $Re_1 = 40$ to $Re_2 = 10$ at $t = 30$, $t = 60$ and $t = 100$. (*b*) As (*a*) but comparing the wake off-centerline vorticity ($\pi - \theta = 0.00592$).

Figure 9(*a*, *b*) compares the two solutions for a sudden decrease in the velocity from $Re_1 = 40$ to $Re_2 = 10$ at $t = 30$, 60 and 100. The parameters are $t_0 = 8$, $x_2 = -1.34$ for $u(x)$ and $x_2 = -3.5$ for ω/y. The motion of the transition zone to the right can be clearly identified. It is noted that the change in the velocity is quite large, $\alpha_{12} = 4$, in this case. The two solutions in the transition zone and the old wake do not agree as well as in the previous two cases in which $\alpha_{12} = \frac{2}{3}$, a relatively mild change. The discrepancy in the old wake is mainly caused by a large x_1 ($x_1 = 18.6$) due to the large α_{12} for the chosen t_0 and x_2.

Figure 10(*a–d*) shows the flow pattern around the sphere when it is suddenly slowed down from $Re_1 = 40$ to $Re_2 = 10$ based on the finite difference solution and the asymptotic solution at $t = 20$ and 50. Instead of seeing a combination of a source at $x \sim 0$ and a sink at $x \sim t$ as in the sudden increase case, we see clearly from both solutions a source of dimensionless volume flux $\hat{Q}_2$ at $x \sim 0$ and a new source in the transition zone, $x \sim t$, of volume flux $(\hat{Q}_1 - \hat{Q}_2)$. The two sources moving apart horizontally as the transition zone continues to move to the right. Figure 11 shows the vorticity contours of the flow field around the sphere with a sudden decrease in the

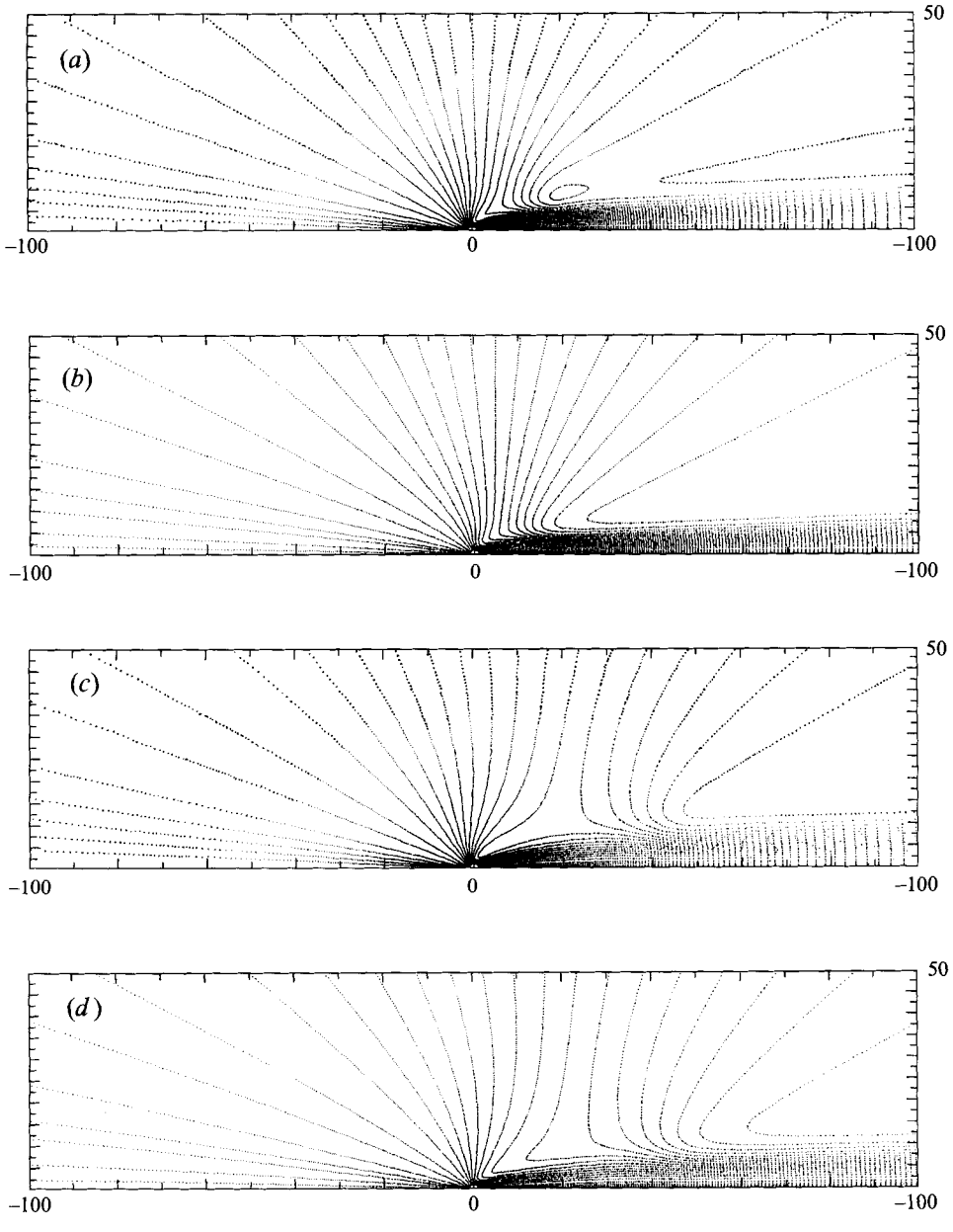

FIGURE 10. Streamlines around a sphere with a sudden decrease in the velocity from $Re_1 = 40$ to $Re_2 = 10$: (*a*) finite difference solution at $t = 20$; (*b*) analytical approximation at $t = 20$; (*c*) finite difference solution at $t = 50$; (*d*) analytical approximation at $t = 50$.

velocity from $Re_1 = 40$ to $Re_2 = 10$ based on the finite difference solution at $t = 20$ and 50. Similar to the sudden increase case from $Re_1 = 40$ to $Re_2 = 60$, the 'discontinuity' in the contours at the transition zone $x \sim t$ can be seen for both $t = 20$ and 50; the vorticity contours near $x \sim t$ are convex for the sudden-decrease case. This corresponds to a 'hole' in the 'vortex pipe' where fluid escapes.

Figure 12(*a*, *b*) compares the flow field around an impulsively stopped sphere based on the finite difference solution with that based on the asymptotic solution given by

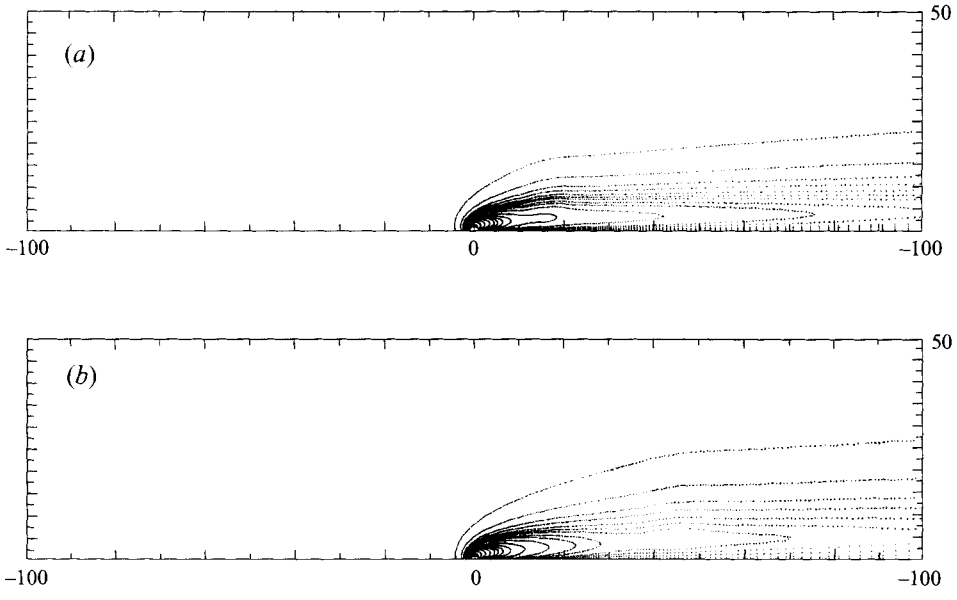

FIGURE 11. Vorticity contours of the flow field around a sphere with a sudden decrease in the velocity from $Re_1 = 40$ to $Re_2 = 10$ based on the finite difference solution. (*a*) $t = 20$; (*b*) $t = 50$.

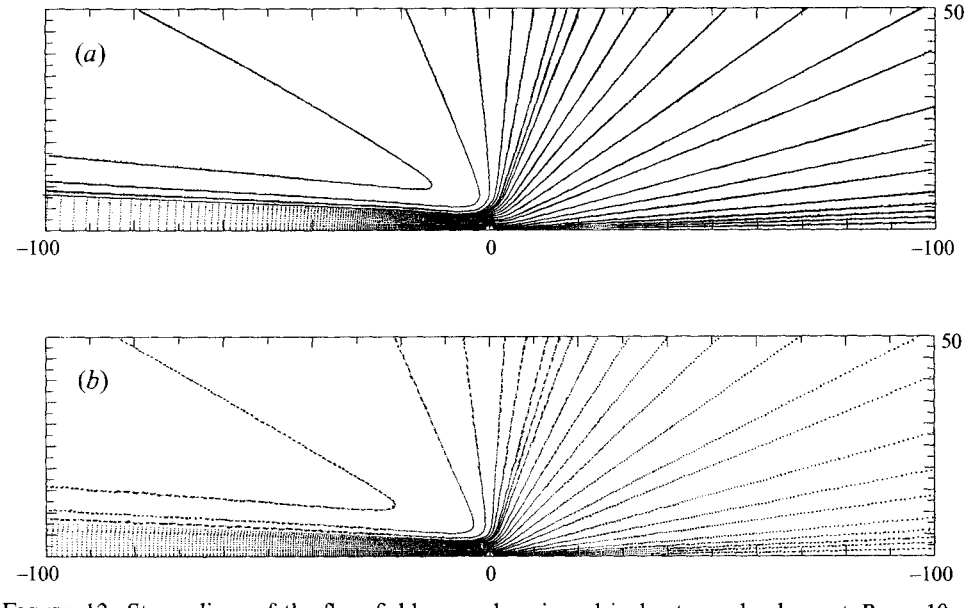

FIGURE 12. Streamlines of the flow field around an impulsively stopped sphere at $Re_1 = 10$ at $t = 15$: (*a*) finite difference solution; (*b*) analytical approximation.

(77) at $t = 15$ with $Re_1 = 10$. Excellent agreement is observed. The sphere originally moves from left to right. On the left, it is seen clearly that the old wake moves toward the sphere and the stream then spreads out through the diffusing source. On the right of the stopped sphere, a source flow is clearly visible. In §2.4, it is pointed out that the volume flux of this source at $x = 0$ is $\hat{Q}_1$ and the source is diffusing out. The diffusion of the source near the sphere has been observed by comparing the spreading of the

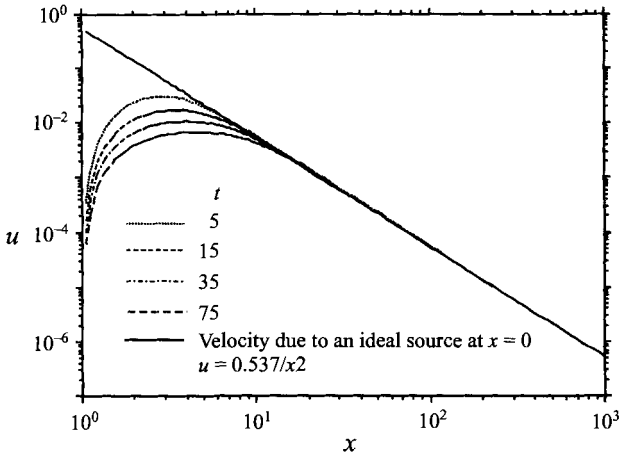

FIGURE 13. Upstream centreline velocity due to an impulsively stopped sphere with $Re_1 = 10$ at $t = 5$, 15, 35 and 75.

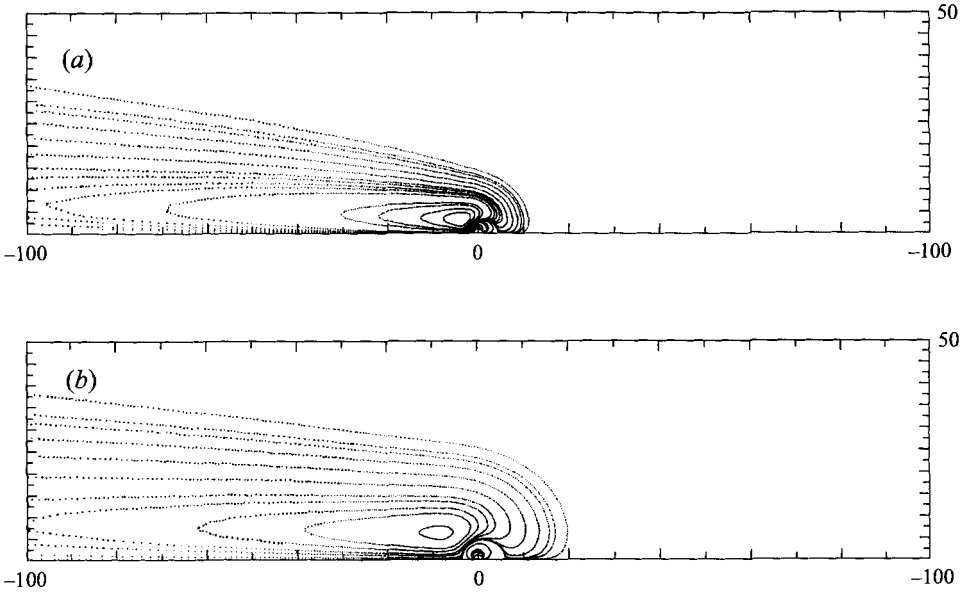

FIGURE 14. Vorticity contours of the flow field around an impulsively stopped sphere with $Re_1 = 10$ based on the finite difference solution. (*a*) $t = 15$; (*b*) $t = 75$.

streamlines from $t = 15$ to 75 (not shown here). To see the diffusing source clearly, figure 13 compares the upstream ($x > 0$) velocity of the impulsively stopped sphere ($Re_1 = 10$) at $t = 5$, 15, 35 and 75 with the idealized source at $x = 0$, $u_{up}^{source}(x) = 0.537/x^2$. For $x > 10$, the flow is still dominated by the source. Near the sphere, the velocity decreases with time as the source diffuses. The spreading of the old wake can be better illustrated by examining the unsteady vorticity contours as shown in figure 14(*a*, *b*) for $t = 15$ and 75. Near the sphere, a new vorticity field is created by the incoming wake flow and interacts with the incoming vorticity of the old wake. Since the velocity of the passing wake becomes weaker, the vorticity near the sphere decreases with time and spreads out through diffusion. Chang & Maxey (1995)

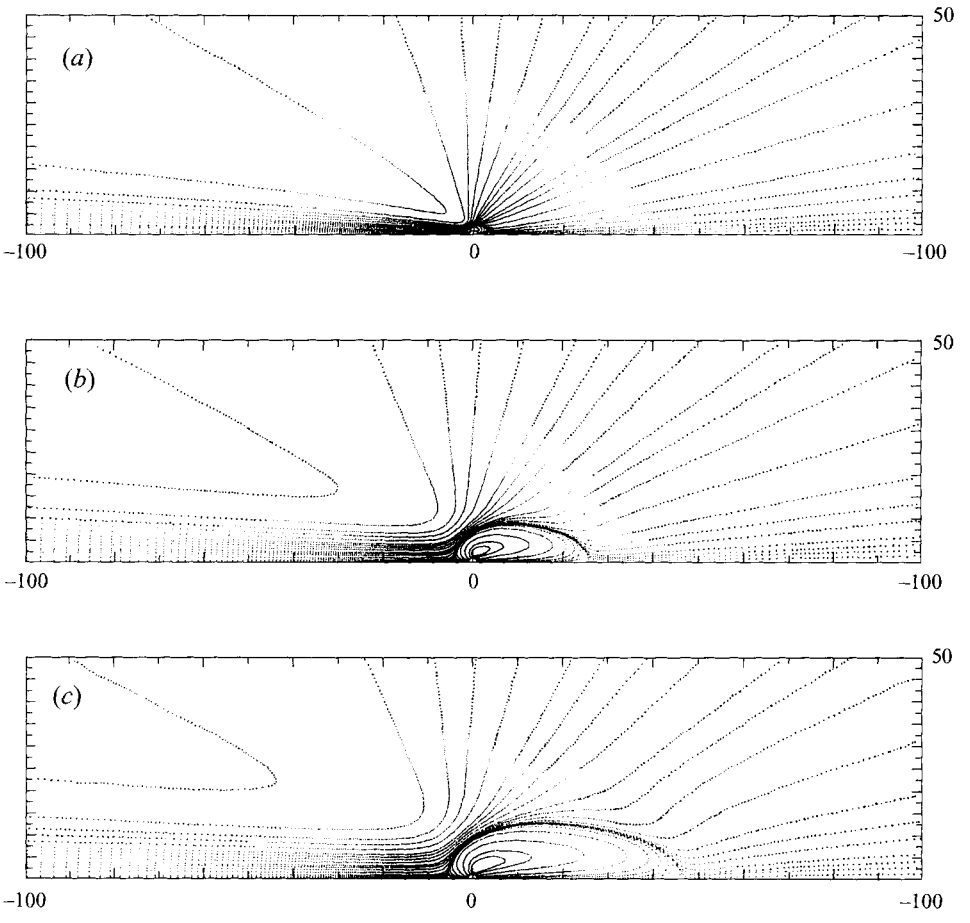

FIGURE 15. Streamlines around an impulsively reversed sphere at $Re_1 = Re_2 = 10$ based on the finite difference solution. (*a*) $t = 0.5$; (*b*) $t = 20$; (*c*) $t = 40$.

presented the streamlines around the sphere in the near field ($|x| \leqslant 9$) soon after the sphere is brought to rest from $R = 10$. Their flow pattern at very short time in the near field clearly possesses essentially the same features as predicted by our asymptotic analysis for the long time and far field: a source within the body and an old wake behind the body.

Figure 15(*a–c*) shows the flow field around an impulsively reversed sphere with $Re_1 = Re_2 = 10$ and $\alpha_{12} = -1$ at $t = 0.5$, 20 and 40. Only numerical solutions are presented here, but the asymptotic solutions have been checked and show very good agreement. The sphere originally moves from left to right with a wake on the left of the sphere; the old wake is still moving toward the right. As discussed in §2.5, the physics associated with the impulsive reverse can be understood by splitting the impulsive reverse into an impulsive stop at $t = 0^-$ and an impulsive start at $t = 0^+$. In figure 15(*a*), it is seen that shortly after the sphere reverses a recirculation zone is created very close to it. Subsequently, this region grows and stretches out as shown in figure 15 (*b*, *c*). A new wake is clearly visible in figure 15(*c*) for $x < t = 40$. Unlike the impulsive-start case in which a sink of volume flux $\hat{Q}_2$ is located at $x \sim t$, no sign of a sink or source at $x \sim t$ is visible. Instead, the streamlines at $t = 20$ and 40 indicate that only a source at $x \sim 0$ is present on a large scale. It is also pointed out in §2.5 that the

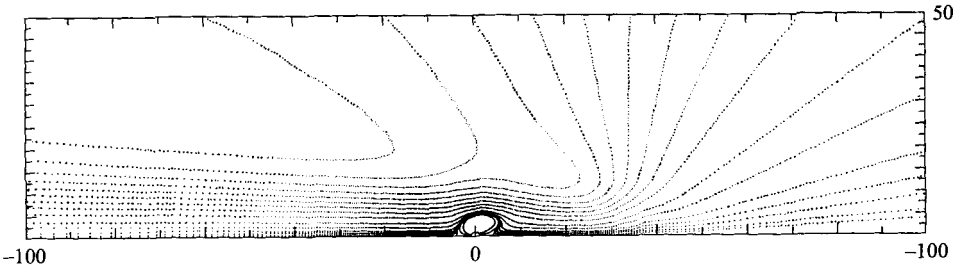

FIGURE 16. The flow due to the diffusing source at $x \sim t$ associated with the impulsive reverse of the sphere. $Re_1 = Re_2 = 10$, $t = 40$.

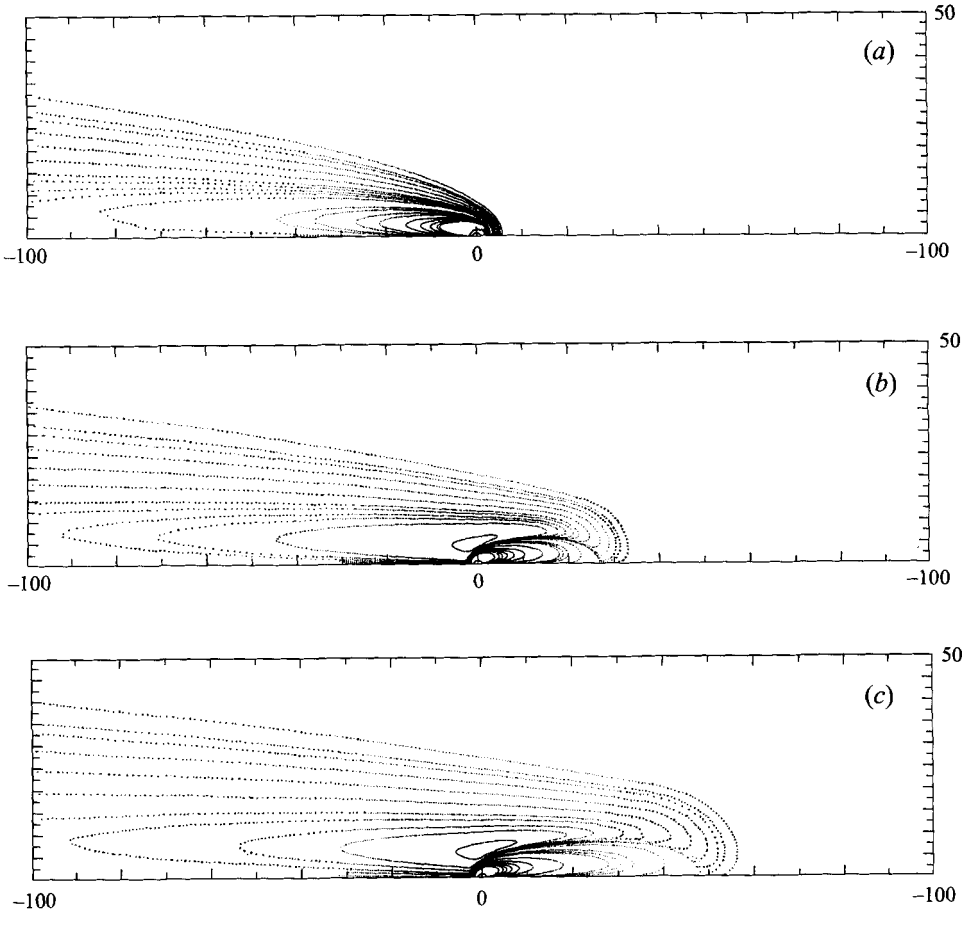

FIGURE 17. Vorticity contours of the flow field around an impulsively reversed sphere at $Re_1 = Re_2 = 10$ based on the finite difference solution (*a*) $t = 0.5$; (*b*) $t = 20$; (*c*) $t = 40$.

sink of flux $\hat{Q}_2$ exactly cancels the effect of the diffusing source of flux $\hat{Q}_1$ at $x \sim t$ that is left after the stopping process. To verify the above analysis, and especially to confirm the presence of the diffusing source $\hat{Q}_1$, we subtract the flow field caused by the impulsive start process with Re_2, which consists of a new source $\hat{Q}_2$ at $x = 0$, a new wake in $0 < x \leqslant t - t_0$, and a sink of flux $\hat{Q}_2$ at $x = t - t_0$, from the numerically obtained flow field. The resulting flow field should mainly contain the old wake and the diffusing

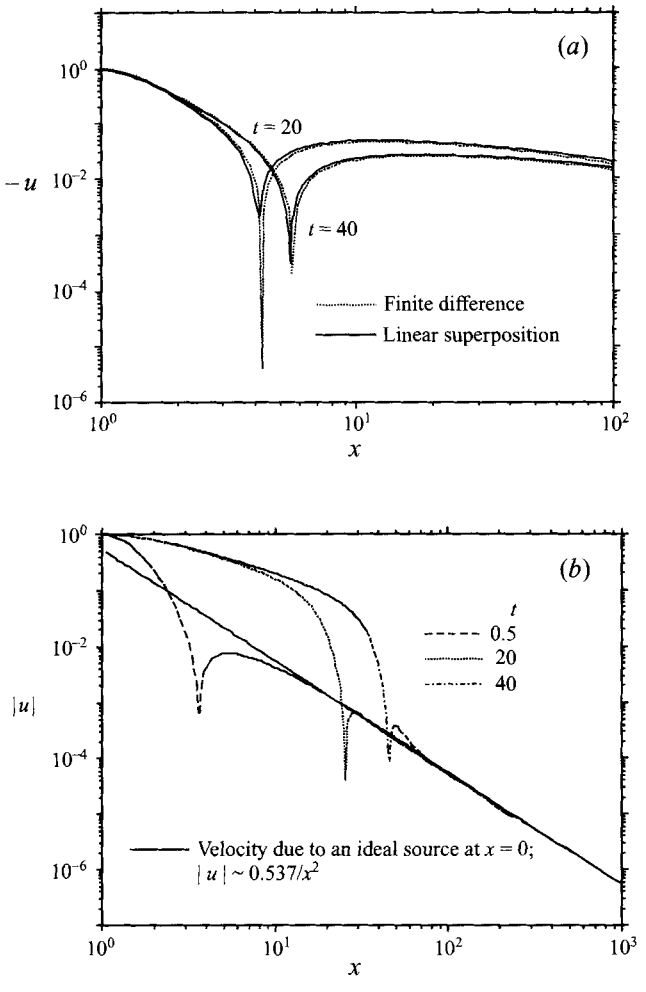

FIGURE 18. (*a*) Upstream velocity due to an impulsively reversed sphere with $Re_1 = Re_2 = 10$ at $t = 20$ and 40. (*b*) Downstream velocity due to an impulsively reversed sphere with $Re_1 = Re_2 = 10$ at $t = 0.5$, 20 and 40 based on the finite difference solution.

source at $x \sim t$ on a large scale, according to the analysis presented in §2.5; the stream function of such a flow field is denoted by ψ_{diff}. Taking $t_0 = 8$, $x_2 = -1.34$, suing the stream function due to the impulsive start similar to (63), ψ_{diff} is easily obtained. Figure 16 shows the contours of ψ_{diff} at $t = 40$. A diffusing source is clearly seen at $x \sim t - t_0 = 32$. To the left of $x \sim t - t_0$, the flow is mainly dominated by the old wake except near the sphere. Near the sphere, $u_{up}^{source}(x)$ does not represent the actual $u_{up}(x)$ well and the linear wake analysis breaks down. Nevertheless, the old-wake/source combination on a large scale is clearly demonstrated. Figure 17(*a–c*) shows the vorticity contours of the flow field around the impulsively reversed sphere at $t = 0.5$, 20 and 40. The interaction of the travelling old wake and the new vorticity field can be clearly observed. The convection of the old wake can also be visualized by laying the ω-contour at $t = 20$ on top of the ω-contour at $t = 40$ and shifting the ω-contour at $t = 20$ to the right by a distance of $(1 - \alpha_{12})(40 - 20) = 40$.

To further understand the complex flow pattern shown in figure 15, we examine the upstream and downstream velocities on the centreline. Figure 18(*a*) shows the

upstream velocity at $t = 20$ and 40 based on the unsteady finite difference solution and the prediction using the steady $u_{up}^{FD}(x)$ and $u_{wake}(x)$ given by (79). Excellent agreement is observed for the velocity, and the front stagnation point is accurately captured by the prediction for $t = 20$ and 40. Figure 18(*b*) shows the downstream velocity at $t = 0.5$, 20 and 40 based on the finite difference solution. Also shown is the velocity due to an ideal source at $x = 0$. By comparing it with figure 3(*a*), it is clear that a new wake has formed between $x \sim 1$ and $x \sim t$. The sink at $x \sim t$ exactly cancels the diffusing source, so that no visible impact is seen. Beyond $x \sim t$, the ideal source $u_{up}^{source}(x)$ clearly dominates. It is also seen that the downstream stagnation point moves as $x_{down} \sim t$ as discussed earlier.

5. Conclusions

The long-time behaviour of the unsteady flow field around a bluff body due to a step change in its travelling velocity from α_{12} to 1 (or in dimensional terms, from U_1 to U_2) has been investigated in detail based on asymptotic analysis and finite difference solution. The step change in the dimensionless velocity includes: (i) an impulsive start with $\alpha_{12} = 0$; (ii) a sudden increase with $0 < \alpha_{12} < 1$; (iii) a sudden decrease with $\alpha_{12} > 1$; (iv) an impulsive stop with $\alpha_{12} \to \infty$ (or $U_1 = 1$ and $U_2 = 0$); and (v) an impulsive reverse with $\alpha_{12} < 0$. For the first three cases, a matched asymptotic solution is obtained to describe quantitatively the unsteady flow structure: a source of volume flux $\hat{Q}_2$ attached to the body, a new quasi-steady wake of volume flux $\hat{Q}_2$ in $0 < x < t$, an old wake of volume flux $\hat{Q}_1$ in the region $x > t$, a sink of volume flux $(\hat{Q}_2 - \hat{Q}_1)$ at the transition zone. For the impulsive stop, the asymptotic analysis for the unsteady flow indicates that it mainly consists of an old wake and a diffusing source of volume flux $\hat{Q}_1$ at $x = 0$. For the impulsive reverse, $\alpha_{12} < 0$, a qualitative analysis reveals the following basic features: (*a*) an old wake in $x < t$ with its apparent origin at $x \sim (1 + |\alpha_{12}|)\, t$; (*b*) a diffusing source of volume flux $\hat{Q}_1$ at $x \sim t$; (*c*) a new source of volume flux $\hat{Q}_2$ at $x \sim 0$, a new wake of volume flux $\hat{Q}_2$ in $0 < x < t$, and a new sink of volume flux $\hat{Q}_2$ at $x \sim t$ (i.e. a net sink of flux $\hat{Q}_2 - \hat{Q}_1$ at $x \sim t$). The basic unsteady flow structures predicted by the analytical approximation agree well with the finite difference solutions for all cases.

In particular, the present study has provided a detailed analysis of the flow fields due to the impulsive stop and reverse to elucidate the unusual t^{-1} behaviour of long-time transient force experienced by the sphere. The findings of the present study, the results of LM, and the analysis of Lovalenti & Brady (1993, 1995) indicate that the long-time behaviour of the history force on a particle in a general unsteady environment at finite Reynolds number is very complicated and problem dependent. Although in practical problems of interest such situations with t^{-1} long-time decay of the transient force are rarely encountered, a generally valid expression for such a force at finite Reynolds number is very difficult to find.

R. M. would like to acknowledge the financial support of the Engineering Research Center (ERC) for Particle Science & Technology at the University of Florida, the National Science Foundation (EEC-9402989), and industrial partners of ERC. C. J. L. acknowledges partial support by a National Science Foundation award CTS 88-57040.

Appendix. Leading-order solution for the transition zone

By dropping terms of $O((\epsilon Re')^{1/2})$ for $\epsilon \ll Re'^{-1}$ or more directly $x \gg Re'$ and $t \gg Re'$, equations (53)–(55) can be simplified to

$$\hat{u}_T = \hat{u}_{RR} + \frac{1}{R}\hat{u}_R + \hat{u}_{\xi\xi} - P_\xi, \tag{A 1}$$

$$V_T = V_{RR} + \frac{1}{R}V_R - \frac{1}{R^2}V + V_{\xi\xi} - P_R, \tag{A 2}$$

$$\hat{\omega}_T = \hat{\omega}_{RR} + \frac{1}{R}\hat{\omega} - \frac{1}{R^2}\hat{\omega} + \hat{\omega}_{\xi\xi}. \tag{A 3}$$

Using $\hat{\zeta} = R\hat{\omega} = R(V_R - \hat{u}_\xi)$, (A 3) becomes

$$\hat{\zeta}_T = \hat{\zeta}_{RR} - \frac{1}{R}\hat{\zeta}_R + \hat{\zeta}_{\xi\xi} \tag{A 4}$$

with the following matching conditions:

$$\xi \to \pm\infty: \quad \hat{\zeta} = -\hat{Q}_{1,2}\frac{1}{8\pi}\frac{R^2}{(T-T_1)^2}\exp\left[-\frac{R^2}{4(T-T_1)}\right]. \tag{A 5}$$

Seeking a solution in the form of

$$\hat{\zeta} = f(R, T)\, g(\xi, T), \tag{A 6}$$

(A 4) becomes

$$g\left(f_{RR} - \frac{1}{R}f_R - f_T\right) = f(g_T - g_{\xi\xi}). \tag{A 7}$$

Taking hints from the matching conditions (A 5), the choice

$$f(R, T) = -\frac{1}{8\pi}\frac{R^2}{(T-T_1)^2}\exp\left[-\frac{R^2}{4(T-T_1)}\right] \tag{A 8}$$

satisfies $f_{RR} - (1/R)f_R - f_T = 0$. Hence, we are left to solve

$$g_T - g_{\xi\xi} = 0 \tag{A 9}$$

with

$$g = \hat{Q}_{1,2} \quad \text{as} \quad \xi \to \pm\infty. \tag{A 10}$$

Anticipating self-similarity, the solution may be obtained as

$$g = \hat{Q}_1 + \tfrac{1}{2}(\hat{Q}_2 - \hat{Q}_1)\,\mathrm{erfc}\,(\tfrac{1}{2}\chi), \tag{A 11}$$

$$\chi = \xi/(T-T_2)^{1/2}, \tag{A 12}$$

where T_2 is a constant of integration and erfc is the complementary error function with $\mathrm{erfc}\,(-\infty) = 2$ and $\mathrm{erfc}\,(\infty) = 0$. Thus,

$$\hat{\zeta} = -\frac{1}{8\pi}\frac{R^2}{(T-T_1)^2}\exp\left[-\frac{R^2}{4(T-T_1)}\right][\hat{Q}_1 + \tfrac{1}{2}(\hat{Q}_2 - \hat{Q}_1)\,\mathrm{erfc}\,(\tfrac{1}{2}\chi)]. \tag{A 13}$$

In general, T_2 could be different from T_1, but for convenience, we set $T_2 = T_1$ so that R and χ are scaled by the same factor $(T-T_1)^{1/2}$. Using η and χ, equation (60) for velocity $\hat{u}$ can be expressed as

$$\frac{1}{\eta}(\eta\hat{u}_\eta)_\eta + \hat{u}_{\chi\chi} = \frac{1}{4\pi(T-T_1)}(1-\tfrac{1}{4}\eta^2)\exp(-\tfrac{1}{4}\eta^2)[\hat{Q}_1 + \tfrac{1}{2}(\hat{Q}_2-\hat{Q}_1)\operatorname{erfc}(\tfrac{1}{2}\chi)], \quad \text{(A 14)}$$

with $\hat{u} = 0$ as $\eta \to \infty$ and the matching conditions given by (57). The solution for $\hat{u}$ may be partitioned in the form of

$$\hat{u} = -\frac{1}{4\pi(T-T_1)}\{\exp(-\tfrac{1}{4}\eta^2)[\hat{Q}_1 + \tfrac{1}{2}(\hat{Q}_2-\hat{Q}_1)\operatorname{erfc}(\tfrac{1}{2}\chi)] + \tilde{u}\} \quad \text{(A 15)}$$

and the remainder $\tilde{u}$ satisfies

$$\frac{1}{\eta}(\eta\tilde{u}_\eta)_\eta + \tilde{u}_{\chi\chi} = (\hat{Q}_2-\hat{Q}_1)\exp(-\tfrac{1}{4}\eta^2)\frac{\chi}{4\pi^{1/2}}\exp(-\tfrac{1}{4}\chi^2) \quad \text{(A 16)}$$

with

$$\tilde{u} = 0 \quad \text{as} \quad \chi \to \pm\infty \quad \text{or} \quad \eta \to \infty. \quad \text{(A 17)}$$

Using local spherical coordinates, $(\chi, \eta) \to (\sigma, \theta)$, with $\chi = \sigma\cos\theta$ and $\eta = \sigma\sin\theta$, (A 16) becomes

$$\frac{1}{\sigma^2}(\sigma^2\tilde{u}_\sigma)_\sigma + \frac{1}{\sigma^2\sin\theta}(\sin\theta\tilde{u}_\theta)_\theta = (\hat{Q}_2-\hat{Q}_1)\frac{1}{4\pi^{1/2}}\sigma\exp(-\tfrac{1}{4}\sigma^2)\cos\theta. \quad \text{(A 18)}$$

Seeking a solution in the form of

$$\tilde{u} = -\frac{1}{4\pi^{1/2}}(\hat{Q}_2-\hat{Q}_1)h(\sigma)\cos\theta, \quad \text{(A 19)}$$

an ordinary differential equation for $h(\sigma)$ results:

$$h'' + \frac{2}{\sigma}h' - \frac{2}{\sigma^2}h = \sigma\exp(-\tfrac{1}{4}\sigma^2) \quad \text{(A 20)}$$

with $h = 0$ as $\sigma \to \infty$. This equation can be integrated directly; the solution is

$$h(\sigma) = \frac{4}{\sigma}\exp(-\tfrac{1}{4}\sigma^2) - \frac{4}{\sigma^2}\pi^{1/2}\operatorname{erf}(\tfrac{1}{2}\sigma). \quad \text{(A 21)}$$

It is noted that $h(\sigma) \sim -\frac{2}{3}\sigma$ as $\sigma \to 0$, and that as $\sigma \to \infty$, $\tilde{u}$ takes the form of a sink of strength $(\hat{Q}_2-\hat{Q}_1)$. Substituting (A 19) and (A 21) into (A 25) gives the velocity $\hat{u}$ in the transition zone:

$$\hat{u} = -\frac{1}{4\pi(T-T_1)}\left\{[\hat{Q}_1 + \tfrac{1}{2}(\hat{Q}_2-\hat{Q}_1)\operatorname{erfc}(\tfrac{1}{2}\chi)]\exp(-\tfrac{1}{4}\eta^2) + (\hat{Q}_2-\hat{Q}_1)\cos\theta\left[\frac{1}{\sigma^2}\operatorname{erf}(\tfrac{1}{2}\sigma) - \frac{1}{\sigma\pi^{1/2}}\exp(-\tfrac{1}{4}\sigma^2)\right]\right\}. \quad \text{(A 22)}$$

Noting that for fixed χ, $\cos\theta = \chi/\sigma$, $\eta\,\mathrm{d}\eta = \sigma\,\mathrm{d}\sigma$ and

$$\left[\frac{1}{\sigma^2}\operatorname{erf}(\tfrac{1}{2}\sigma) - \frac{1}{\sigma\pi^{1/2}}\exp(-\tfrac{1}{4}\sigma^2)\right]\mathrm{d}\sigma = -\mathrm{d}\left[\frac{1}{\sigma}\operatorname{erf}(\tfrac{1}{2}\sigma)\right],$$

the stream function $\hat{\psi}$ in the transition zone, $\hat{\psi}^{TZ}$, can be obtained by integrating $\eta\hat{u}$ with respect to η:

$$\hat{\psi}^{TZ}(\chi,\eta) = -\frac{1}{2\pi}[1-\exp(-\tfrac{1}{4}\eta^2)][\hat{Q}_1+\tfrac{1}{2}(\hat{Q}_2-\hat{Q}_1)\operatorname{erfc}(\tfrac{1}{2}\chi)]$$

$$-\frac{1}{4\pi}(\hat{Q}_2-\hat{Q}_1)[\operatorname{erf}(\tfrac{1}{2}\chi)-\cos\theta\operatorname{erf}(\tfrac{1}{2}\sigma)]. \quad \text{(A 23)}$$

It is seen that for fixed η

$$\hat{\psi}^{TZ}\to-\frac{1}{2\pi}[1-\exp(-\tfrac{1}{4}\eta^2)]\hat{Q}_2 \quad \text{as} \quad \chi\to-\infty \qquad \text{(A 24}a\text{)}$$

and

$$\hat{\psi}^{TZ}\to-\frac{1}{2\pi}[1-\exp(-\tfrac{1}{4}\eta^2)]\hat{Q}_1 \quad \text{as} \quad \chi\to+\infty. \qquad \text{(A 24}b\text{)}$$

This is consistent with (41*b*) and (42*b*). The radial component of the velocity V can be obtained, if desired, by differentiating $\hat{\psi}^{TZ}$.

REFERENCES

BATCHELOR, G. K. 1967 *An Introduction to Fluid Dynamics*. Cambridge University Press.

CHANG, E. J. & MAXEY, M. 1995 Unsteady-flow about a sphere at low to moderate Reynolds number. Part 2. Accelerated motion. *J. Fluid Mech.* **303**, 133–153.

LAWRENCE, C. J. & MEI, R. 1995 Long-time behaviour of the drag on a body in impulsive motion. *J. Fluid Mech.* **283**, 307–327 (referred to herein as LM).

LOVALENTI, P. & BRADY, J. 1993 The hydrodynamic force on a rigid particle undergoing arbitrarily time-dependent motion at small Reynolds number. *J. Fluid Mech.* **256**, 561–605.

LOVALENTI, P. & BRADY, J. 1995 The temporal behavior of the hydrodynamic force on a body in response to an abrupt change in velocity at small but finite Reynolds-number. *J. Fluid Mech.* **293**, 35–46.

MEI, R. 1993 History force on a sphere due to a step change in the free-stream velocity. *Intl J. Multiphase Flow*, **19**, 509–525.

MEI, R. 1994 Flow due to an oscillating sphere and an expression for unsteady drag on the sphere at finite Reynolds number. *J. Fluid Mech.* **270**, 133–174.

MEI, R. & ADRIAN, R. J. 1992 Flow past a sphere with an oscillation in the free-stream and unsteady drag at finite Reynolds number. *J. Fluid Mech.* **237**, 323–341.

MEI, R., KLAUSNER, J. F. & LAWRENCE, C. J. 1994 A note on the history force on a spherical bubble at finite Reynolds number. *Phys. Fluids* A **6**, 418–420.

MEI, R. & PLOTKIN, A. 1986 Navier–Stokes solution for some laminar incompressible flows with separation in forward facing step geometries. *AIAA J.* **24**, 1106–1111.

PEDLEY, T. J. 1975 A thermal boundary layer in a reversing flow. *J. Fluid Mech.* **75**, 209–225.

SCHLICHTING, H. 1979 *Boundary Layer Theory*, 7th Edn. McGraw-Hill.